The cryptic stratigraphic record of the syn- to post-rift transition in the offshore Campos Basin, SE Brazil

Francyne Bochi do Amarante[1,#]

[1] Instituto de Geociências, Universidade Federal do Rio Grande do Sul, Porto Alegre, 90650 001, Brazil

[#] corresponding author francyne.amarante@ufrgs.br

ORCID https://orcid.org/0000-0003-4452-8635

Juliano Kuchle[1]

[1] Instituto de Geociências, Universidade Federal do Rio Grande do Sul, Porto Alegre, 90650 001, Brazil

juliano.kuchle@ufrgs.br

ORCID https://orcid.org/0000-0003-4325-0547

Christopher Aiden-Lee Jackson[2,3]

[2] Jacobs, Manchester, M15 4GU, United Kingdom

[3] Basins Research Group (BRG), Department of Earth Science and Engineering, Imperial College London, London, SW7 2BP, United Kingdom

christopher.jackson@manchester.ac.uk

ORCID https://orcid.org/0000-0002-8592-9032

Claiton Marlon dos Santos Scherer[1]

[1] Instituto de Geociências, Universidade Federal do Rio Grande do Sul, Porto Alegre, 90650 001, Brazil

claiton.scherer@ufrgs.br

ORCID https://orcid.org/0000-0002-7520-1187

Leonardo Muniz Pichel[4]

[3] Department of Earth Science, University of Bergen, 5007, Bergen, Norway

leonardo.m.pichel@uib.no

ORCID https://orcid.org/0000-0001-8692-3831

This manuscript is a preprint and has been submitted for publication in **Basin Research**. Please note that this manuscript has not yet undergone peer-review; as such, subsequent version of this manuscript may have different content. We invite you to contact any of the authors directly to comment and give any feedbacks on the manuscripts.

Abstract

Rift basins typically comprise three main tectono-stratigraphic stages; pre-, syn-, and post-rift. The syn-rift stage is characterized by the deposition of asymmetric wedges of growth strata that record differential subsidence caused by active normal faulting. The subsequent post-rift stage is defined by long-wavelength subsidence driven by lithospheric cooling, and is typified by the deposition of broadly tabular stratal packages that drape any rift-related relief. The stratigraphic contact between syn- and post-rift rocks is often expressed as an erosional unconformity. However, the late syn-rift to early post-rift stratigraphic record is commonly far more complex since: (i) the associated tectonic transition is not instantaneous; (ii) net-subsidence may be punctuated by transient periods of uplift; and (iii) strain often migrates oceanward during rifting and continental breakup. The marginal basins of southeastern Brazil, including the Campos Basin, have not historically used the tripartite scheme outlined above, with the post-pre-rift interval instead being subdivided into rift, sag, and passive margin tectono-stratigraphic stages. The sag stage has been previously described as late syn-rift, early post-rift, or as a transition between the two, with the passive margin stage being equivalent to the classically defined post-rift stage. Two (rather than one) erosional unconformities are also identified within the rift-to-sag succession. We here use 2D and 3D seismic reflection and borehole data to discuss the expression of and controls on the syn- to post-rift transition in the south-central Campos Basin, offshore southeast Brazil. We mapped three intervals bounded by unconformities. The Barremian - lower Aptian interval is characterized by wedge-shaped packages of reflections that thicken towards graben and half-graben-bounding normal faults. This stage ends with a development of an angular unconformity, inferred to form during the onset of the oceanward migration of deformation. The upper Aptian interval is subdivided into two units; the pre-salt and salt. The pre-salt is typically

defined by packages of subparallel and relatively continuous reflections that are broadly lenticular and thin towards fault-bound basement highs, but that locally diverge towards rift-related normal faults. The pre-salt to salt contact is defined by an erosional unconformity that is largely restricted to basement highs, and which is inferred to have formed due to base-level fall and uplift associated with local fault reactivation. Based on their geometries and seismic facies, we conclude that the Barremian – lower Aptian interval is syn-rifting and *syn-tectonic*, deposited during active continental extension and upper crustal faulting affecting the entire evolving margin, whereas the overlying upper Aptian interval is syn-rifting and *post-tectonic*, deposited when extension and faulting had migrated seaward to the future location of plate rupture and ocean development. The results of our study support the arising notion that the tripartite tectono-stratigraphic model for rift development is too simplistic and cannot be applied when assessing rifts in the context of the regional development of continental margins.

Keywords: pre-salt reservoirs, sag basin, rift basin, South Atlantic basins, continental margins, unconformity.

1. Introduction

The tectonic evolution of rift basins and the rifting process comprise three main tectono-stratigraphic stages; pre-, syn-, and post-rift. Classical models of rift basin evolution are based on the analysis of the sedimentary record preserved within individual grabens and half-grabens; studies such as these typically allow the timing and duration of these stages to be constrained (e.g. Prosser, 1993; Bosence, 1998; Gawthorpe and Leeder, 2000). In these models, the syn-rift stage is characterized by mechanical subsidence, marked by the generation of large amounts of accommodation over a relatively short

period. Mechanical subsidence occurs due to slip on normal faults movement and the associated rotation of intervening fault blocks, resulting in differential subsidence and the formation of grabens or half-grabens, separated by horsts (i.e. basement highs). During this time (named *mid syn-rift* by Bosence, 1998, and *rift climax* by Prosser, 1993 and Kuchle and Scherer, 2010), the greatest thickness of sediment accumulates next to the half-graben border fault; in the case of a symmetrical graben, sediment thicken across the bounding faults, into the intervening depocentre. Active faulting gradually decreases and ceases (Gawthorpe and Leeder, 2000), and mechanical subsidence is replaced by a long-wavelength, relatively slow subsidence driven by cooling of the lithosphere (Prosser, 1993; Bosence, 1998). In some cases, this transition is associated with plate rupture, the steady-state emplacement of oceanic crust (i.e., oceanic spreading) which leads to greater thermal subsidence by cooling of the newly formed magmatic crust and exhumed mantle, and the formation of rifted margins (see below; see also Bott, 1995). When this does not occur, a so-called "failed rift" develops (Allen and Allen, 2005).

Idealised models for rift basin development agree on the gross definition and character of these tectono-stratigraphic stages, but they diverge as where to position the syn- to post-rift transition within this framework. Bosence (1998) considers the syn-rift only ends once the rift-related depocentres are filled with sediments and the associated rift topography is "healed"; the top of the syn-rift succession is defined by the post-rift unconformity, which in marginal basins corresponds to the breakup unconformity (*sensu* Falvey, 1974). Gawthorpe and Leeder (2000) broadly follow the model of Bosence (1998), and highlight that the final syn-rift stage (which the authors designate as *fault death stage*) is characterized by an intense erosion the footwalls, related to the decrease in tectonic activity and the resultant stabilisation of syn-rift drainage systems. Prosser (1993) proposes that the syn-rift ends when the mechanical subsidence associated with

rifting ceases (following previous studies of Cartwright, 1991; see also Nottvedt et al., 1995). Consequently, the post-rift includes passive infilling of any relict rift-related relief, and Prosser (1993) does not describe an unconformity between the syn- and post-rift. Morley (2002) highlights the difficulty of defining the end of the syn-rift stage in his model using the observations of Prosser (1993), showing that the sedimentary fill associated with active faulting can have the same stratigraphic architecture (i.e., across-fault thickening) as a succession that simply fills an inactive, sediment-starved hanging-wall.

Determination of the timing and stratigraphic position of the late syn-rift to early post-rift boundary becomes even more complex if one extrapolates the tripartite scheme established for rift basins to rifted margins, given that during the latter is often associated with: (i) a tectonic transition that is not instantaneous; (ii) net-subsidence that may be punctuated by transient periods of uplift; and (iii) the oceanward migration of strain (e.g. Peron-Pinvidic et al., 2013; Brune et al., 2014; Pérez-Gussinyé, 2020; Chenin et al., 2021). The multistage rifting model for rifted margins (*sensu* Chenin et al., 2021) defines different domains associated with sequential periods of active deformation, and characterized by specific tectonic structures and related stratigraphic architectures. In this model, the term *syn-rift* refers to the *temporal* dimension of the rift event, i.e., from the onset of crustal extension, to plate rupture and the steady-state emplacement of oceanic crust. This stage can then be subdivided into pre-, syn- and post-tectonic (*sensu* Péron-Pinvidic et al., 2007), based on the architecture of sedimentary deposits with respect to local tectonic structures and their activity.

The marginal basins of southeastern Brazil, including the Campos Basin, have not historically used the tripartite scheme outlined above by Prosser (1993) and others, with the syn- and post-rift intervals instead being subdivided into three tectono-stratigraphic

stages: rift, sag and passive margin (or drift) (e.g. Rangel et al., 1994; Winter et al., 2007; Mohriak et al., 2008). Because of the reasons outlined above, there is no consensus on where to position the sag stage within the rifting process. Some authors consider it to be post-rift (Winter et al., 2007; Alvarenga et al., 2021), whereas others position it within the late syn-rift (Karner and Gamboa, 2007; Torsvik et al., 2009). Some authors even argue it constitutes an additional, *transitional stage* between the syn- and post-rift, with the passive margin stage being equivalent to the classically defined post-rift stage (Rangel et al., 1994; Beglinger et al., 2012; Cainelli and Mohriak, 1999). Variable interpretations of the tectono-stratigraphic framework of the south-eastern Brazilian margin may reflect uncertainties related to the number and character of rift-related unconformities (especially the breakup unconformity; *sensu* Falvey, 1974). Two (rather than one) erosional unconformities have been recognized in the southeastern Brazilian basins. The first occurs between the rift and the sag stages and is known as the *pre-Alagoas* (or *pre-neo-Alagoas*) unconformity, which is dated at 120 – 123 Ma (intra-Aptian; Winter et al., 2007; Mohriak et al., 2008). Some authors argue that this unconformity records breakup of the South Atlantic continental crust, and that therefore marks the end of the syn-rift (e.g. Cainelli and Mohriak, 1999; Mohriak et al., 2008). A second erosional unconformity occurs between the sag pre-salt sediments and the salt (Winter et al., 2007; Karner and Gamboa, 2007; Alves et al., 2017). The origin of this unconformity is uncertain; for example, Karner and Gamboa (2007) attribute it to base-level fall, lake desiccation, and subaerial erosion during the late syn-rift, whereas Alves et al. (2017) partially attribute it to a combination of subaerial exposure and shear traction at the base of flowing salt during gravity-driven tectonics, with ridge push-related uplift as an additional tectonic driver.

In this study, we use 2D and 3D seismic reflection and borehole date to characterize the syn-rift tectono-stratigraphic architecture and the geometry and nature of its main unconformities, in particular the that marks the syn- to post-rift transition in the south-central Campos Basin, offshore southeast Brazil. We detail three, post-pre-rift intervals – *Barremian - lower Aptian*, *upper Aptian salt* and *upper Aptian pre-salt* – and their bounding surfaces. We subsequently discuss the origin of the mapped stratigraphic surfaces, correlating them between proximal and distal parts of the margin. Finally, we define the pre-, syn-, and post-rift tectono-stratigraphic stages within a multistage rifting model.

2. Geological Context

The Campos Basin originated during the rifting process that led to the breakup of Gondwana, and which culminated in the opening of the South Atlantic Ocean in the Upper Jurassic/Lower Cretaceous (Szatmari, 2000). The basin occupies c. 115,000 km², and it is located on the southeastern Brazilian margin, offshore the states of Espírito Santo and Rio de Janeiro (Figure 1a). The northern boundary between Campos and Espírito Santo basin is defined by the Vitória High, whereas the southern boundary with Santos Basin is marked by the Cabo Frio High (Mohriak et al., 1989).

The stratigraphy of the Campos Basin can be broadly divided into three tectono-stratigraphic or megasequences (rift, sag, and passive margin), although it should be noted that this and the associated age constraints are widely debated (Figure 1b) (e.g. Tedeschi et al., 2019; Strugale and Cartwright, 2022; Szatmari et al.,2021). The rift sequence initiated at c. 135 Ma with the intense volcanic activity that emplaced basaltic and volcanoclastic rocks of Cabiúnas Formation (Baksi, 2018). The sedimentary sequence of

the rift stage (Barremian – early Aptian) comprises the basal and intermediate intervals of the Lagoa Feia Group (Winter et al., 2007), characterized by lacustrine deposits (interbedded with the volcanoclastics of Cabiúnas Formation), including alluvial conglomerates and sandstones, organic-rich shales, and bioclastic rudstones and grainstones thought to be deposited within "coquinas" (Abrahão and Warme, 1990; Rangel et al., 1994, Goldberg et al., 2017). Rifting was accommodated by NE-SW-striking normal faults that dip to the NW or SE, and which bound structural highs (horsts) and lows (grabens) (Dias et al., 1988; Chang et al., 1992, Alvarenga et al., 2021), including the Badejo, Intermediate and External highs, and the Corvina-Parati and External lows (Figure 2a; Guardado et al., 2000). The marginal hinge line of the rift system is delineated by the Campos fault (Figure 2a), which separates the shallow western part, where Tertiary deposits rest directly on basement, from the deeper eastern portion, where relatively thick accumulations of Barremian to Aptian sediments fill rift-related depocentres (Guardado et al., 1989).

The sag sequence (upper Aptian) marks the transition from mechanical subsidence, induced by basement-involved faulting to thermal subsidence, to a period characterized by longer-wavelength subsidence, driven by cooling of the lithosphere, and little normal faulting (Guardado et al., 1989). This sequence is dated between 116 – 123 Ma (Karner and Gamboa 2007; Moreira et al., 2007), becoming progressively older from the proximal to distal parts of the basin (Pérez-Gussinýe et al., 2020). The shift in subsidence style is recorded by a regional unconformity (*i.e.* the pre-Alagoas unconformity, as named by Guardado et al., 1989) and by an enlargement in depositional area as sedimentation progressively 'healed' rift topography (Quirk et al., 2013; Kukla et al., 2018; Amarante et al., 2020). The sedimentary succession of the sag stage of the Campos Basin comprises the upper Lagoa Feia Group (Figure 1b), which is characterized

by clastic sediments in proximal parts of the basin, and microbial and chemically precipitated carbonates in more distal areas, which are together overlain by a thick layer of evaporites (Dias et al. 1988; Winter et al., 2007, Herlinger et al., 2017).

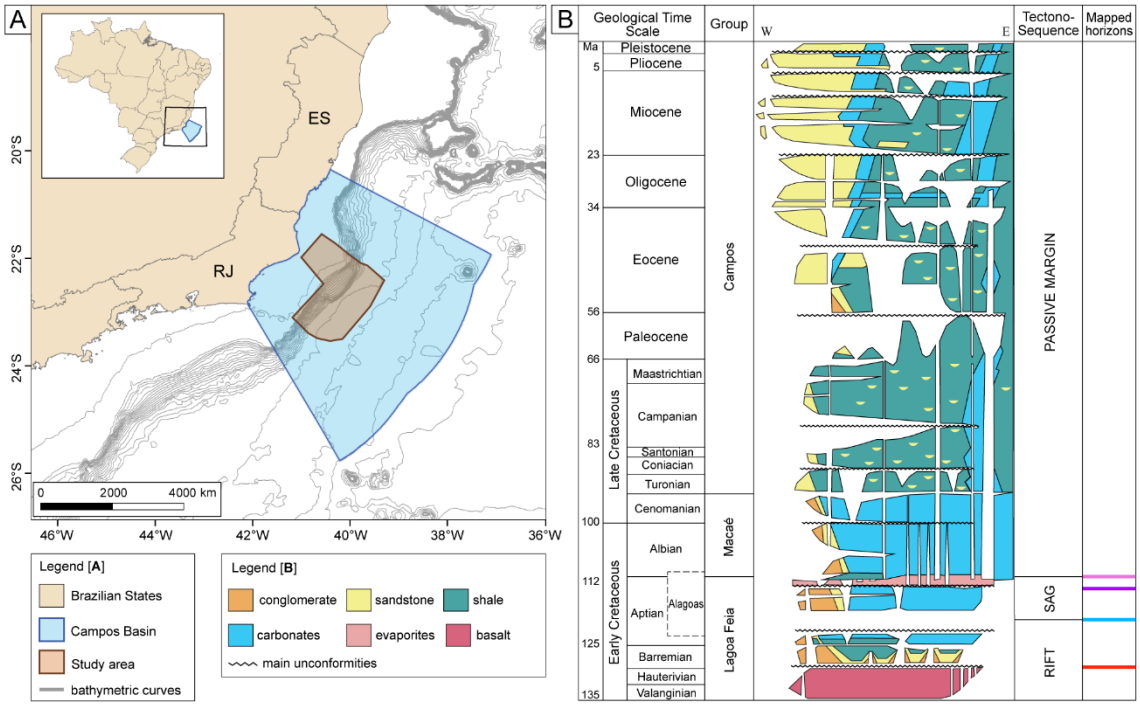

Figure 1. (A) Regional map showing the location of Campos Basin and the study area polygon highlighted in brown (B) Simplified stratigraphic chart of Campos Basin, subdivided into three tectono-sequences: rift, sag and passive margin (redrawn from Winter et al., 2007); the column to the right shows the mapped horizons of this study with their designed colours.

The passive margin sequence marks the start of oceanic spreading and the development of the Mid-Atlantic Ridge (Winter et al., 2007). The initiation of drift deposition is associated with a marine transgression in the upper Cretaceous, recorded by shallow-water carbonate platforms of the Macaé Group (Albian – Cenomanian), overlain by a sequence of pelagic and hemipelagic mudstone and turbidities of the Campos Group (Turonian – Present; Chang et al., 1992). The Macaé and Campos groups are separated by a regional erosional unconformity 93 Ma (Figure 1b; Guardado et al., 1989). The focusing of thermally induced subsidence near the location of continental breakup caused the basin to tilt to SE, inducing gravity gliding of the Aptian salt and its overburden (Quirk et al., 2012). Based on the structural style of salt and its overburden, the Campos Basin is

divided into three domains of salt-related deformation: (i) a proximal extensional domain, associated with the formation of listric normal faults, rafts, and salt rollers; (ii) a distal contractional domain, characterized by salt-cored anticlines and diapirs; and (iii) an intermediate multiphase domain, dominated by hybrid extensional/compressional structures and ramp syncline basins (Amarante et al., 2021).

It is important to note that the ages of the syn-rift and sag sequences, and the lowermost units in the passive margin sequence, are debated. A relatively recent publication (Tedeschi et al., 2019) presented high-resolution, carbon isotope ($\delta^{13}C$) data from basins along the eastern Brazilian margin, correlating them with well-calibrated Tethyan sections. These new correlations conclude that major evaporite deposition in the South Atlantic occurred in the early Aptian (124 – 125 Ma), suggesting the underlying pre-salt sag sequence is approximately late Barremian and the deeper-still rift sequence is approximately Hauterivian – lower Barremian (Strugale and Cartwright, 2022 – see their figure 2). However, these new age constraints for the salt were recently challenged by Szatmari et al. (2021), who suggest the eastern Brazilian basins evolved in a different paleoenvironmental and thus faunal realm to the Tethyan section, meaning a correlation between the two is problematic. Instead, Szatmari et al. (2021) use ^{39}Ar–^{40}Ar dating to propose that the South Atlantic evaporites (and related volcanic rocks) are c. 116 – 110 Ma (i.e., latest Aptian-earliest Albian).

Plate reconstructions show that the onset of seafloor spreading in the southern Campos Basin occurred during the late Aptian (c. 115 Ma; Heine et al., 2013; Moulin et al., 2013). This means that the sag sequence (pre-salt and salt) can be either pre-, syn- or post-breakup, depending on whether the age constraints of Tedeschi et al. (2019) or Szatmari et al. (2021) are considered correct. Considering what is most accepted in plate

reconstructions, the sag interval is pre- to syn-breakup (e.g. Heine et al., 2013; Perez-Gussinye et al, 2020; Kukla et al., 2018).

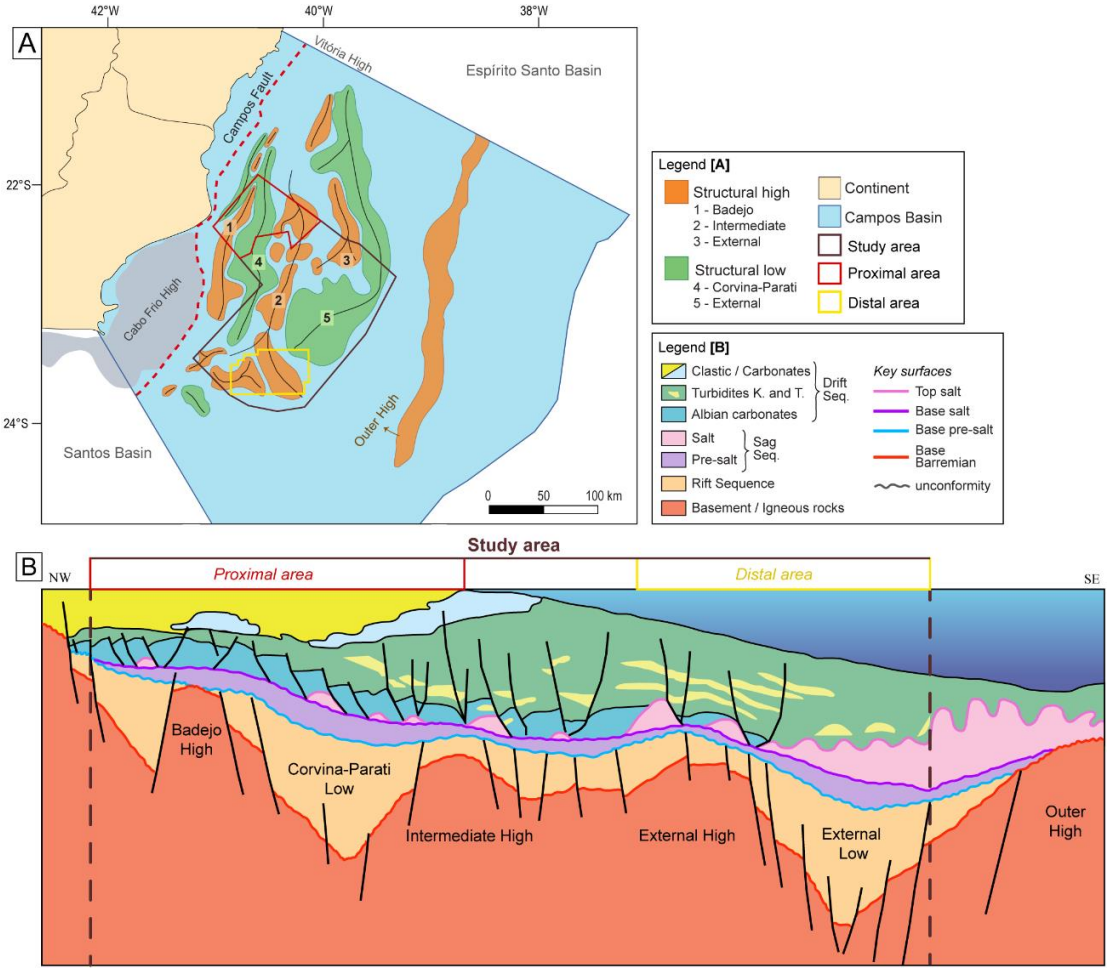

Figure 2. (A) Rift-related structural framework of Campos Basin, the structural highs (horsts) are colored in orange, and the structural lows (grabens), in green. Redrawn from Guardado et al. (2000); the Outer High and Cabo Frio High locations are from Fetter (2009). (B) Schematic cross section of Campos Basin, showing the rift-related structures present in the detailed proximal and distal portions within the study area (see Figure 3). Redrawn and modified from Rangel et al., 1994.

3. Database and Methodology

The database for this study comprises 209 2D seismic reflection lines (or line segments), one 3D seismic reflection volume, and 33 wells from the ANP (Brazil's National Oil, Natural Gas and Biofuels Agency) data library. In total, the 2D seismic surveys cover an area of c. 23,300 km² (Figure 3). The 3D volume covers an area of c.

2,900 km² in the southern part of the study area, with inline (east-west) and crossline (north-south) spacing of 12.5 m. The seismic surveys are time-migrated (PSTM Kirchoff), zero-phase processed, and are displayed with SEG normal polarity, where a downward increase in acoustic impedance is represented by a positive reflection event (white on displayed seismic profiles) and a downward decrease in acoustic impedance is represented by a negative reflection event (black on displayed seismic profiles). All seismic data (lines and maps) are presented in miliseconds (ms) two-way travel time (TWT).

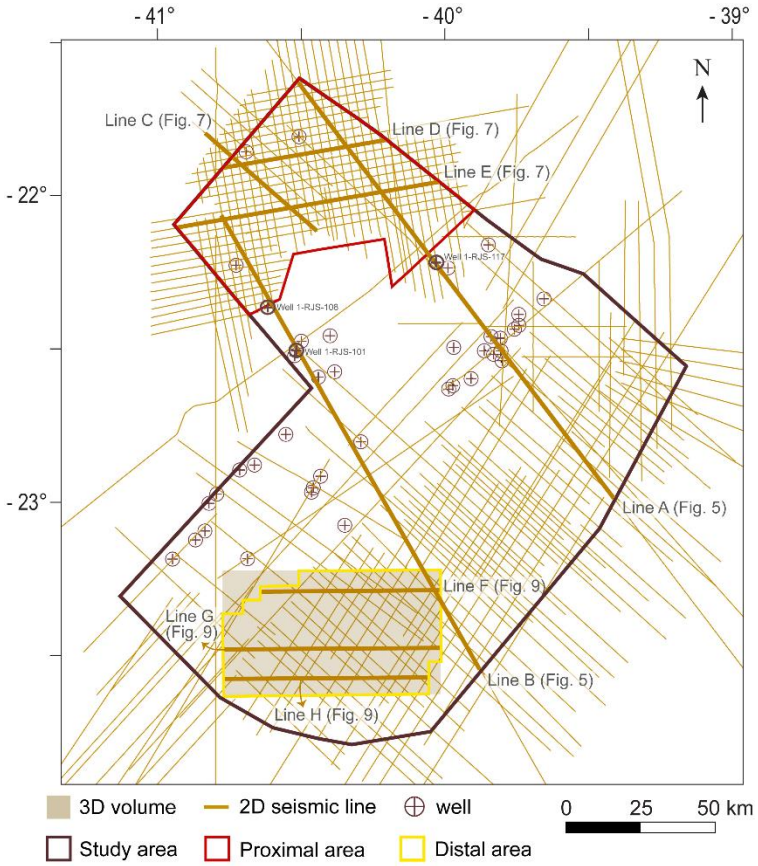

Figure 3. Dataset used in this study: 209 2D seismic lines (or lines segments), one 3D volume and 33 boreholes. The red and yellow polygons represent the proximal and distal areas (respectively) which have greater data density – and, therefore, are discussed in detail within the paper. Note the label of the lines presented in figures 5, 7 and 9, and the wells 1-RJS-108, 1-RJS-101 and 1-RJS-117 presented in figure 5.

The 33 boreholes include well-logs (e.g. sonic travel time and gamma ray), stratigraphic (age and formation tops) and cuttings-based lithological data, used to constrain the age, composition, and lithostratigraphy of the mapped horizons and the units

they bound. These wells were tied to the seismic data through check-shot surveys. The interval velocity of the Aptian evaporites obtained from the well-logs ranges from 4000 – 7000 m/s, depending on the proportion of halite, anhydrite, and potash salts. The sedimentary succession below the salt is defined by interval velocities ranging from 3100 – 6000 m/s due to the varying densities and porosities of the different lithologies (e.g. sandstones, carbonates, mudstones). We estimate that the vertical seismic resolution in the interval of interest is 25 – 50 m; more specifically, 30 – 50 m within the salt (using a dominant frequency of 35 Hz), and 25 – 50 m within the underlying strata (considering a dominant frequency of 30 Hz).

We identified four key stratigraphic surfaces in the study area, with age constraints provided by well data: early Barremian (top of Cabiúnas Fm.), mid Aptian unconformity, late Aptian unconformity (base of the salt), and top Aptian (top of the salt). The last three were mapped across the entire dataset (Figure 1b). We also selected two areas with greater data density and quality, one proximal and one distal (Figure 3), where we also mapped the base Barremian (top of Cabiúnas Fm.) surface. The four mapped horizons bound three intervals: *Barremian - lower Aptian*, *upper Aptian salt* and *upper Aptian pre-salt*. The mapped surfaces display the present basin geometry, whereas isochron maps derived from these surfaces reflect the relative thickness of the intervals; the latter are used to infer temporal and spatial changes in subsidence and accommodation, which might relate to some combination of tectonics and sea-level change (Figures 4, 6 and 8). The absolute thickness values presented in the text were calculated by converting time (TWT, ms) to depth using velocities of 4700 m/s and 5100 m/s – i.e. the average interval velocity of the pre-salt and salt intervals, respectively, calculated from the well-logs. We also calculated the dip-angle of the base-pre-salt and base-salt surfaces using the same methodology.

4. Basement structures

The study area comprises the following basement structures, from the proximal to the distal portions: the Corvina-Parati Low, the Badejo High, the Intermediate and External highs, and the External basement lows (Figures 2 and 5). These structures are grabens and horsts bounded by rift-related normal faults. The External High is present only to the northeast portion (Figure 5a).

Proximal area

The proximal area contains the Corvina-Parati Low and the Badejo and Intermediate highs, which are both bounded by N-S- to NE-SW-striking normal faults that are up to 55 km long and that have throws of up to 1500 ms TWT. The Corvina-Parati Low is bound to the southeast by the Intermediate High and to the northwest by the Badejo High, which extends north-westwards until the Campos Fault, the marginal hinge line of the basin (Figures 6a and 7). The Corvina-Parati Low contains two depocenters, which have mean depths between -3500 and -5000 ms TWT, and which are dissected by the Badejo High (Figures 6a and 7). The Badejo High is not as deeply buried as the Intermediate High (c. -3050 to -1600 ms TWT compared to, c. -3700 ms to -2900 ms TWT; Fig. 6a).

Distal area

The distal area contains the External High to the west and the External Low to the east, bounded by N-S- to NNE-SSW-striking normal fault, that are up to c. 40 km long and have throws of up to 800 ms TWT. The External High varies in depth between -4600 and -5800 ms TWT (Figure 8a) and it is characterized by a series of normal faults with relatively small vertical displacement (up to 400 ms TWT), delimiting restricted, asymmetric depocenters (Figure 9). The base of the External Low is at -7400 ms TWT

(Figure 8a), and it contains a series of antithetic and synthetic faults that define depocenters separated by internal basement highs (Figure 9b,c).

5. Barremian – lower Aptian

The base-Barremian horizon separates the chaotic reflections of the basement and syn-rift volcanics (which we are not able to differentiate) from divergent to subparallel reflections of the sedimentary succession (Figure 5). The top of this interval is defined by an erosional unconformity that is best-developed near basement highs, and which is characterised by truncation of tilted reflections (Figures 7 and 9).

Proximal area

The base-Barremian in the proximal area varies in depth from -1650 to -4900 ms TWT (Figure 6a). Sedimentation in this interval is mainly restricted to a largely isolated depocentre within the Corvina-Parati Low. The depocenter to the NW is a half-graben, containing high-frequency reflections that occur in a wedge-shaped package that thickens towards the border fault. The depocenter to the SE is a relatively symmetric graben, containing subparallel, lower frequency reflections (Figure 7). On the Intermediate High are isolated, asymmetric depocentres containing divergent reflections (Figure 7c).

Distal area

The base of the Barremian in the distal area varies between -4450 and -7300 ms TWT depth (Figure 8a). Like in the proximal area, sedimentation is restricted to single depocenters that are isolated from adjacent ones by elevated basement structures. Within grabens and half-grabens of the External Low, reflections are divergent to subparallel, locally folded and disrupted, and have relatively high frequencies and medium to high

amplitude. In restricted depocentres within the External High, the reflections are divergent to subparallel, and are of low to medium amplitude and of relatively low frequency (Figure 9).

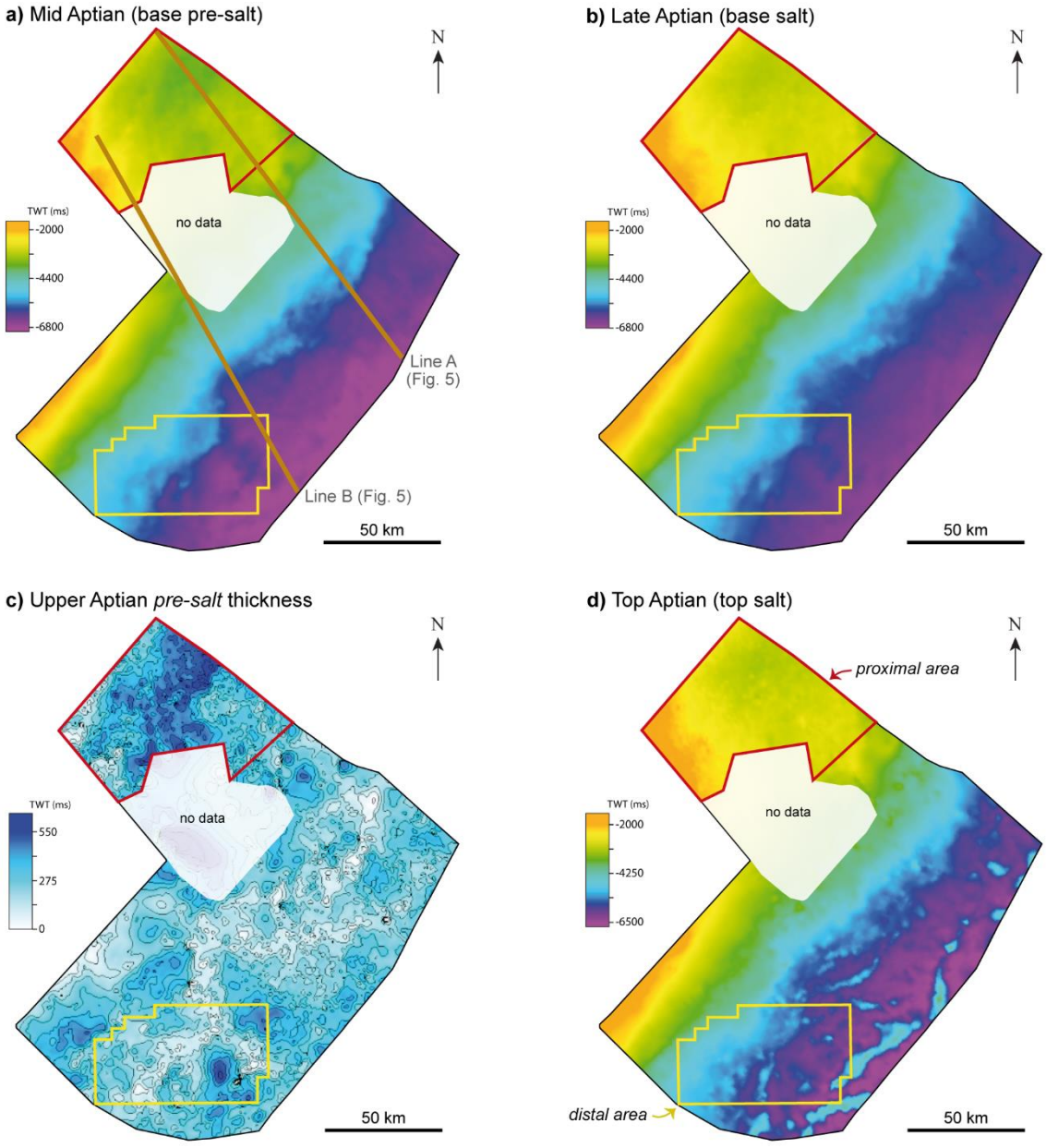

Figure 4. Time map of the mid Aptian (base pre-salt) (a) and late Aptian (base salt) (b) surfaces of the entire study area, which vary from -1600 – -7000 and -1550 – -6800 ms (TWT), respectively, and dip regionally to SE. The seismic lines shown in figure 5 are indicated in brown. c) Pre-salt (Upper Aptian) isochron thickness map, showing values from 0 –675 ms (TWT); thickness is overall greater in the proximal area (red polygon). d) Time map of the top Aptian (top salt) surface, varying from -1500 and -6700 ms (TWT). The area with very few data (see Figure 3) is indicated in white.

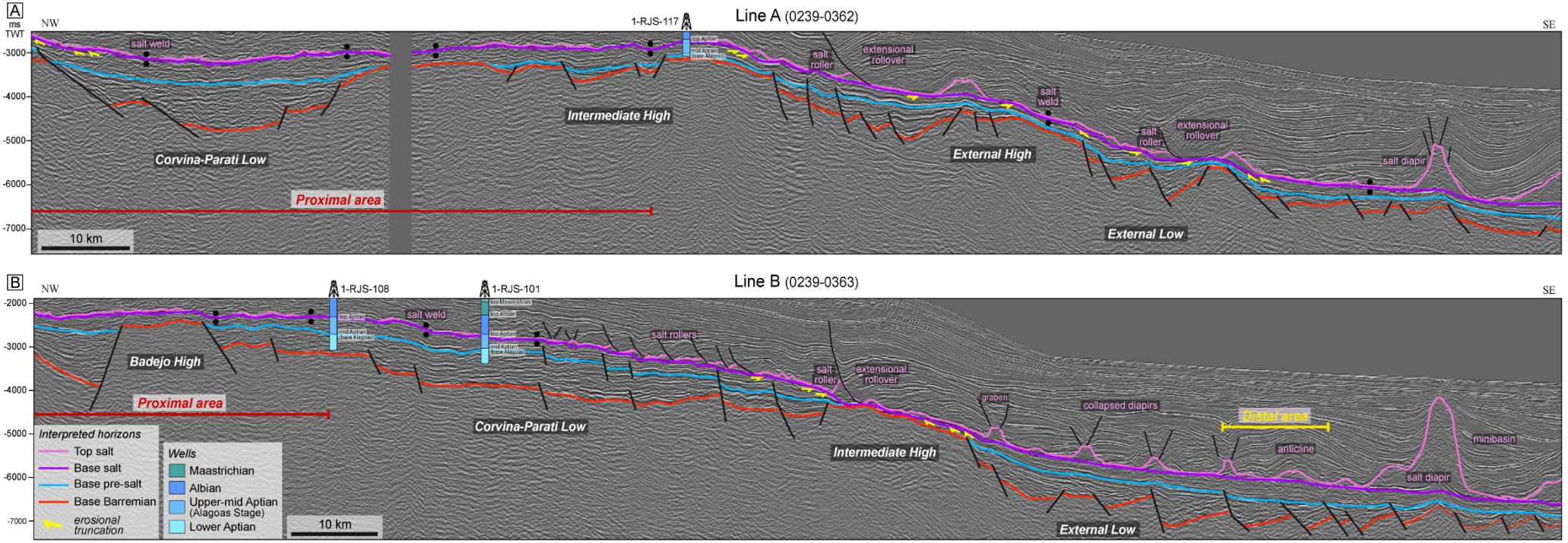

Figure 5. Regional lines of the study area (see figures 3 and 4a for location). The interpreted horizons are indicated in the legend in the lower left corner. Reflection terminations in erosional truncations are highlighted with yellow arrows. There are three wells with age constraints, 1-RJS-117 intersected by Line A, and wells 1-RJS-0108 and 1-RJS-0101 intersected by Line B. The main salt and overburden structures are labelled in pink. The basement highs and lows (see figure 2) are labelled, as well as the proximal and distal areas.

6. Upper Aptian

6.1. Pre-salt interval

The base-pre-salt surface varies in depth between -1600 and -7000 ms TWT and dips regionally to SE (Figure 4a); within basement lows, this surface is defined by a continuous reflection that onlaps locally against the larger basement highs or normal faults (Figure 5). The pre-salt thickness ranges from 0 – 675 ms TWT (c. 0 – 1580 m), and it is overall greater in the proximal portion (Figure 4c). In general, the reflections within this interval are subparallel and relatively continuous (Figure 5).

Proximal area

The base-pre-salt surface varies in depth from -1700 to -3800 ms TWT, and has a mean dip of 3.5° to SE. The pre-salt thickness in the proximal area varies from 0 to 670 ms TWT (c. 0 – 1570 m) (Figure 6d). At the base of the succession, reflections onlap against the basement highs or the basal pre-salt surface. The external geometry of this succession is lenticular, thinning toward the basement highs and thickening within the lows (Figure 7). The reflections are overall parallel to subparallel, except towards the west where they are slightly divergent between the Badejo High and the Corvina-Parati Low (Figure 7b).

Distal area

The depth of the base-pre-salt surface ranges from -4300 to -6900 ms TWT, and has an average dip of 4° to SE (Figure 8b). The pre-salt thickness in the distal area varies from 0 to 570 ms TWT (c. 0 – 1340 m) and is greatest within the External Low (Figure 8d). The reflections are mostly continuous and parallel to subparallel, but divergent reflections are also present towards some of the normal faults (see numbered faults in

Figure 9). The base of the succession is characterized by onlaps against the basement highs or the basal surface (i.e. the base-pre-salt) (Figure 9).

6.2. Salt – pre-salt contact

The salt – pre-salt contact (i.e. base-salt surface) lies between a depth range of -1550 to -6800 ms TWT, dipping regionally towards the SE (Figure 4b). The base-salt surface is rugose, defined by a high-amplitude continuous reflection, underlain by either concordant or tilted reflections; in the latter case, the base-salt surface defines an erosional unconformities (Figure 5). Between the Intermediate/External highs and the External Low, where the surface is erosional, it is best-described as a downcutting erosional unconformity, i.e., underlying reflections are gently dipping, with the overlying erosional surface cutting down into them more steeply (Figure 5).

Proximal area

The depth of the base-salt surface ranges between -1600 and -3500 ms TWT of depth, and dips 2.5° to SE (Figure 6b,c). The salt – pre-salt contact is defined by an erosional unconformity, especially on basement the Badejo High (Figures 7 and 10a). On the Intermediate High and the Corvina-Parati Low, concordant reflections dominate and the base-salt surface is apparently conformable, at least at the scale of observation permitted by the seismic reflection data. Erosionally truncated reflections locally define channel-like seismic facies in the top pre-salt (Figure 10a3) or small incisions at base-salt surface (Figure 10 a2), but they are mostly are unidirectional towards the basement high (Figures 7 and 10 a4). Locally there are truncations within basement lows, in general related to minor faulting (Figure 10a1). The magnitude of erosion at the base-salt

53 increases towards basement highs where the pre-salt is relatively thin and locally absent
54 (Figure 6d).

55 ***Distal area***

56 The depth of the base-salt surface ranges from -3900 to -6400 ms TWT, and has
57 an average dip of 3.5° towards SE (Figure 8c). In a similar manner to that observed in the
58 proximal area, the salt – pre-salt contact can defines a downcutting erosional
59 unconformity on basement highs (Figure 9a to the W and Figure 10 b4 to N), apparently
60 passing laterally into a correlative conformity in adjacent lows (Figures 9 and 10b). Figure
61 10 b3 shows a channel-like incision measuring 4.5 km, 250 ms TWT high. In a similar
62 manner to the proximal area, the magnitude of erosion at base-salt increases towards the
63 basement highs (Figures 9 and 10 b1, b4).

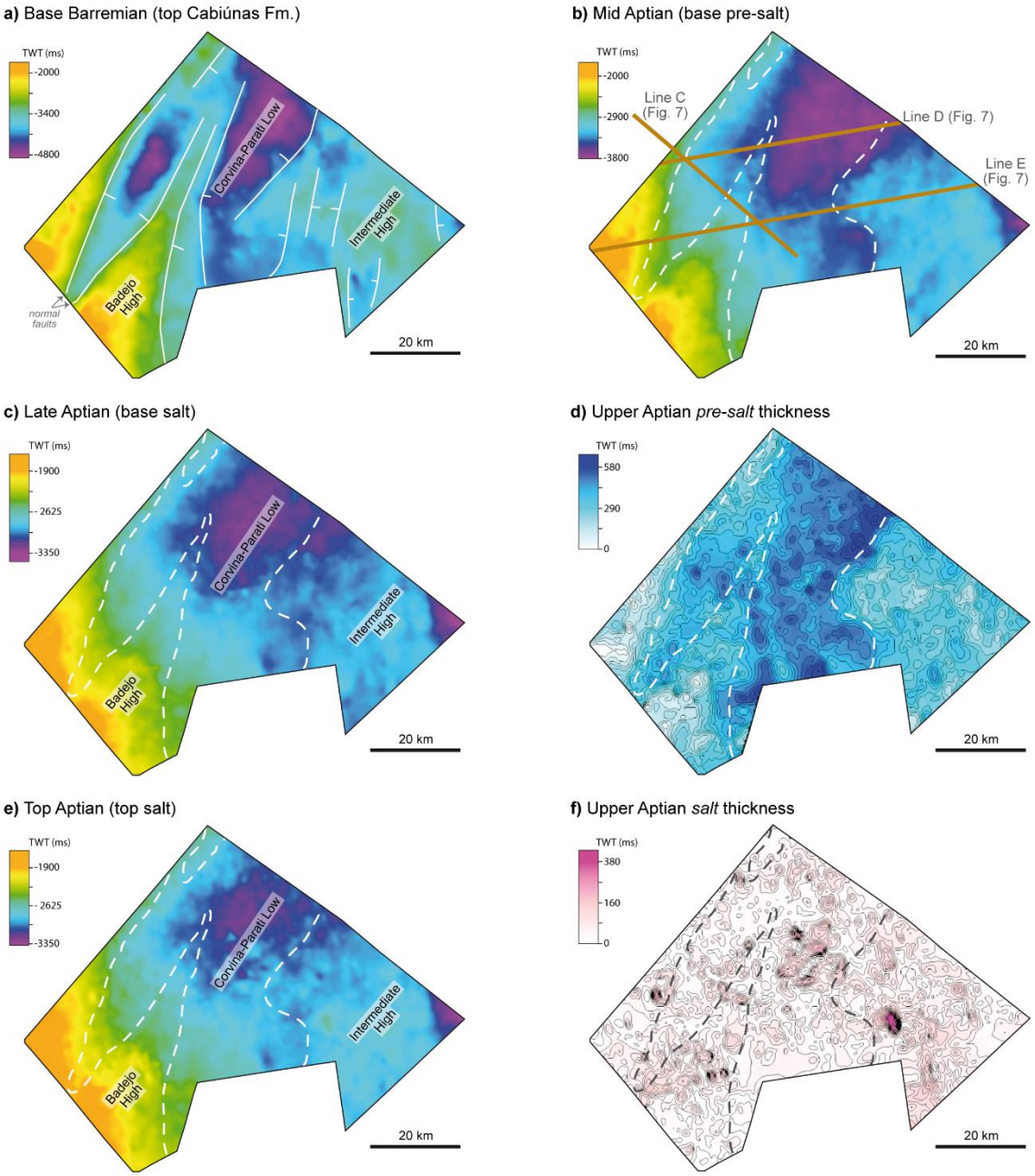

Figure 6. Time maps of the proximal study area. a) Time map of the base Barremian (top Cabiúnas Formation) surface, with values that range from -1650 to -4900 ms (TWT); normal faults delineated in white define basement highs (Badejo and Intermediate) and low (Corvina-Parati) – see figure 2. b) Time map of the mid Aptian (base pre-salt) surface, which varies from -1700 to -3800 ms (TWT). The seismic lines shown in figure 7 are indicated in brown. c) Time map of the late Aptian (base salt) surface, ranging from -1600 and -3500 ms (TWT). d) Pre-salt (upper Aptian) isochron thickness map, with values up to 670 ms (TWT), greater in the Corvina-Parati basement low in comparison to the basement highs. e) Time map of the top Aptian (top salt) surface, with values that range from -1550 to -3400 ms (TWT). f) Salt isochron thickness map, with values ranging from 0 to 425 ms (TWT) defining salt welds and salt structures. The white/black dashed lines contour basement highs and lows.

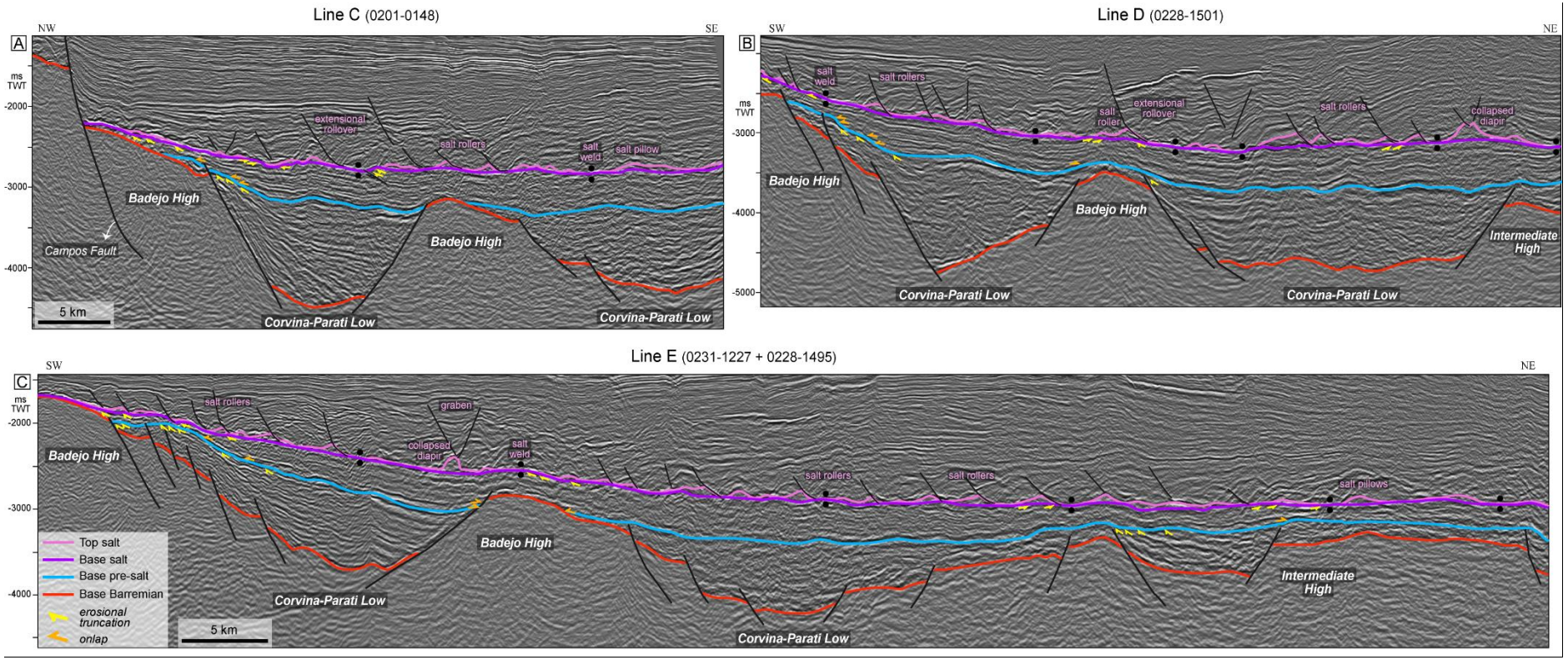

Figure 7. Interpreted lines segments of the proximal area within the study area (see figures 3 and 6b for location of the lines). The interpreted horizons are indicated in the legend in the lower left corner. The main salt and overburden structures are labelled in pink. Reflection terminations in erosional truncations and onlaps are highlighted with yellow and orange arrows, respectively; note how they concentrate to the west, towards the marginal hinge line of the rift system.

6.3. Aptian salt

The top salt surface ranges in depth from -1500 to -6700 ms TWT, and it dips regionally to SE (Figure 4d). The morphology of the top salt surface defines a range of salt structures, including rollers, pillows, diapirs, and anticlines, and numerous related overburden structures such as extensional rollovers, grabens, normal faults, ramp-syncline basins, anticlines, and minibasins (Figures 5, 7 and 9). Salt structures are flanked by salt welds (i.e., areas of relatively thin, depleted salt); in these regions, sub- and supra-salt strata appear to be in direct contact. The distribution and structural style of salt and its overburden, and the geometry of related growth strata preserved within ramp-syncline basins, document substantial horizontal translation (i.e., 28 km; Amarante et al., 2021; see also Dooley et al., 2017).

Proximal area

The top-salt surface varies in depth from -1550 to -3400 ms TWT (Figure 6e). Salt is relatively thin in this area (0 – 100 ms TWT or c. 0 – 250m), being thickest (up to 425 ms TWT or c. 1080 m) in a few, relatively isolated salt structures such as rollers, or more rarely pillows and collapsed diapirs. The salt isochron map shows that the structures are either circular or elongated with a NE to N trend (Figure 6f). Salt structures are typically associated with normal faults overlain by extensional rollovers and/or grabens (Figure 7).

Distal area

The top-salt surface ranges between -3900 and -6350 ms TWT in depth (Figure 8e). Salt thickness is highly variable in this area, 0 – 2500 ms TWT (c. 0 – 6375 m) (Figure 8f). Salt structures trend broadly NE to N, sub-parallel to the underlying rift structures (Figure 8a,f). Over the External High, the salt has flowed to form rollers and collapsed diapirs associated with normal faults that define grabens and extensional turtle

anticlines in the overburden (Figure 9). Structures above the External Low include salt anticlines, rollers, and diapirs (Figure 9).

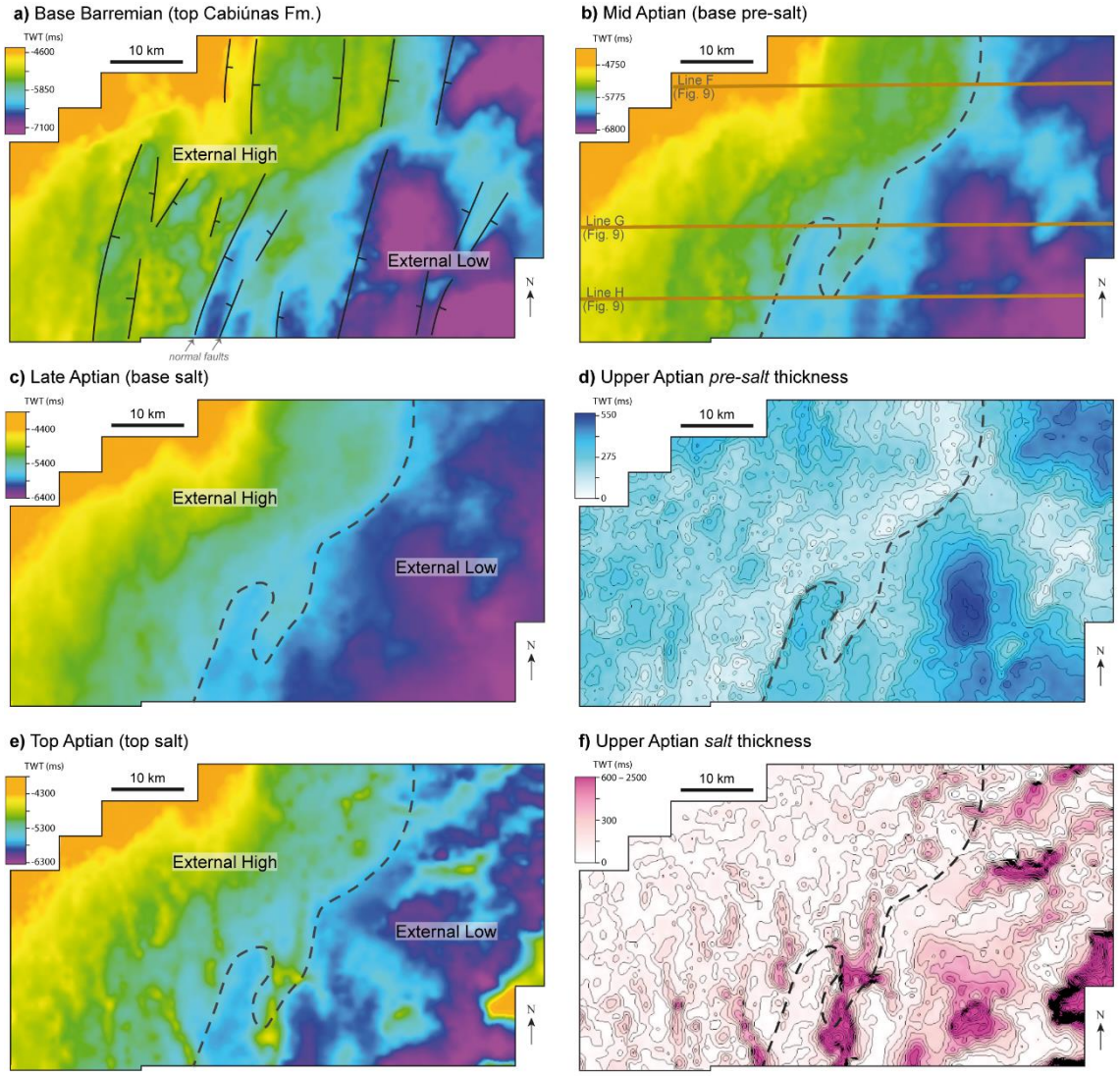

Figure 8. Time maps of the distal study area. a) Time map of the base Barremian (top Cabiúnas Formation) surface, with values that range from -4450 and -7300 ms (TWT); normal faults delineated in black define the basement External High and External Low – see figure 2. b) and c) are time maps of the mid Aptian (base pre-salt) and late Aptian (base-salt) surfaces, which vary from -4300 to -6900 and -3900 to -6400 ms (TWT), respectively. The seismic lines shown in figure 9 are indicated in brown. d) Pre-salt (upper Aptian) isochron thickness map, with values up to 570 ms (TWT), greater in the External Low in comparison to the External High. e) Time map of the top Aptian (top salt) surface, with values that range from -3900 to -6350 ms (TWT). f) Salt isochron thickness map, with values ranging from 0 to 2500 ms (TWT) defining salt welds and salt structures. The black dotted line bounds the basement high and low.

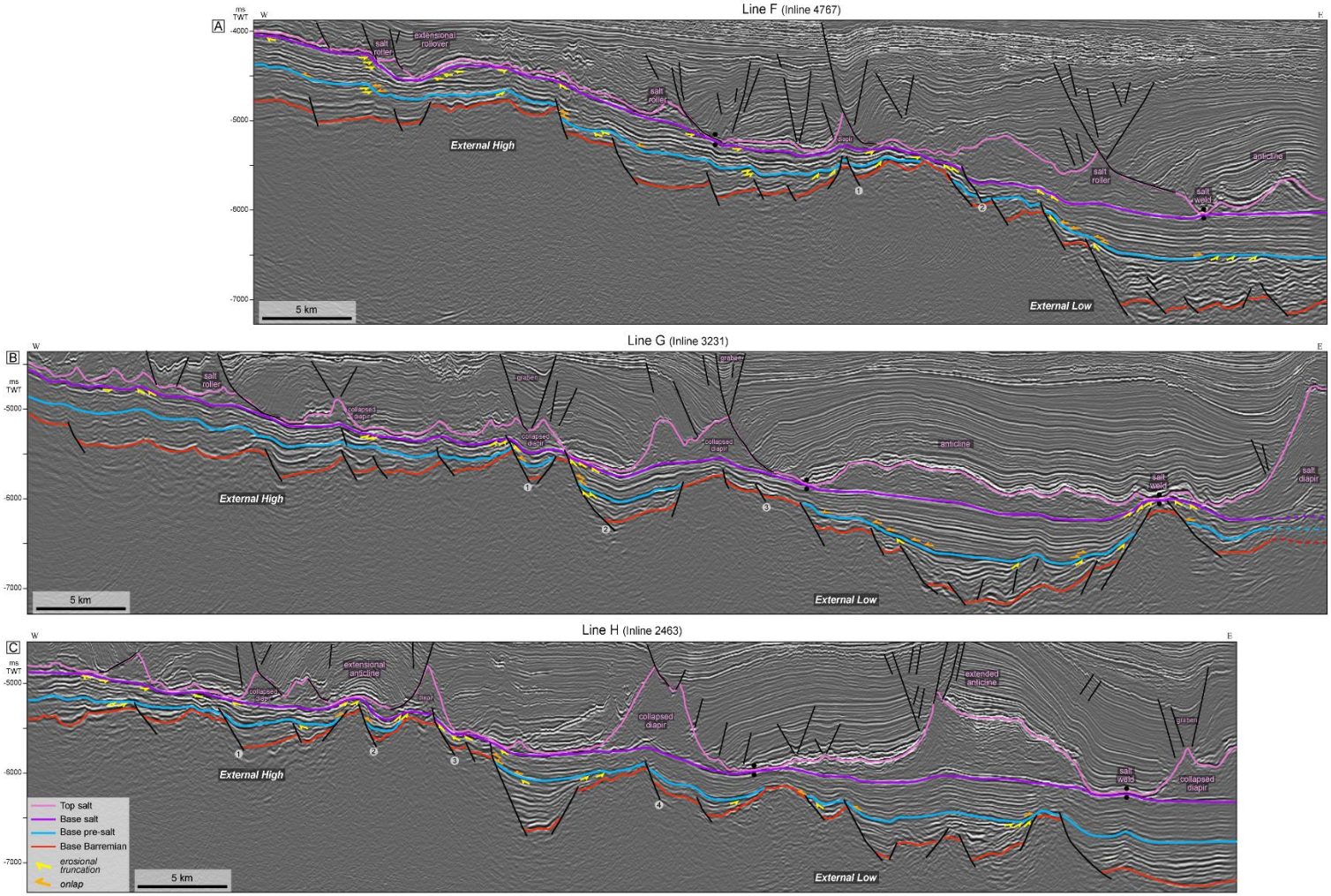

Figure 9. Interpreted lines of the distal area (3D volume) within the study area (see figures 3 and 8b for location of the lines). The interpreted horizons are indicated in the legend in the lower left corner. The main salt and overburden structures are labelled in pink. The faults that were active during the pre-salt interval (upper Aptian) are numbered. Reflection terminations in erosional truncations and onlaps are highlighted with yellow and orange arrows, respectively; note how they concentrate to the west, in the External High and in the boundary between the External High and the External Low. In (b) and (c) there are also erosional truncations near the internal basement high to the east.

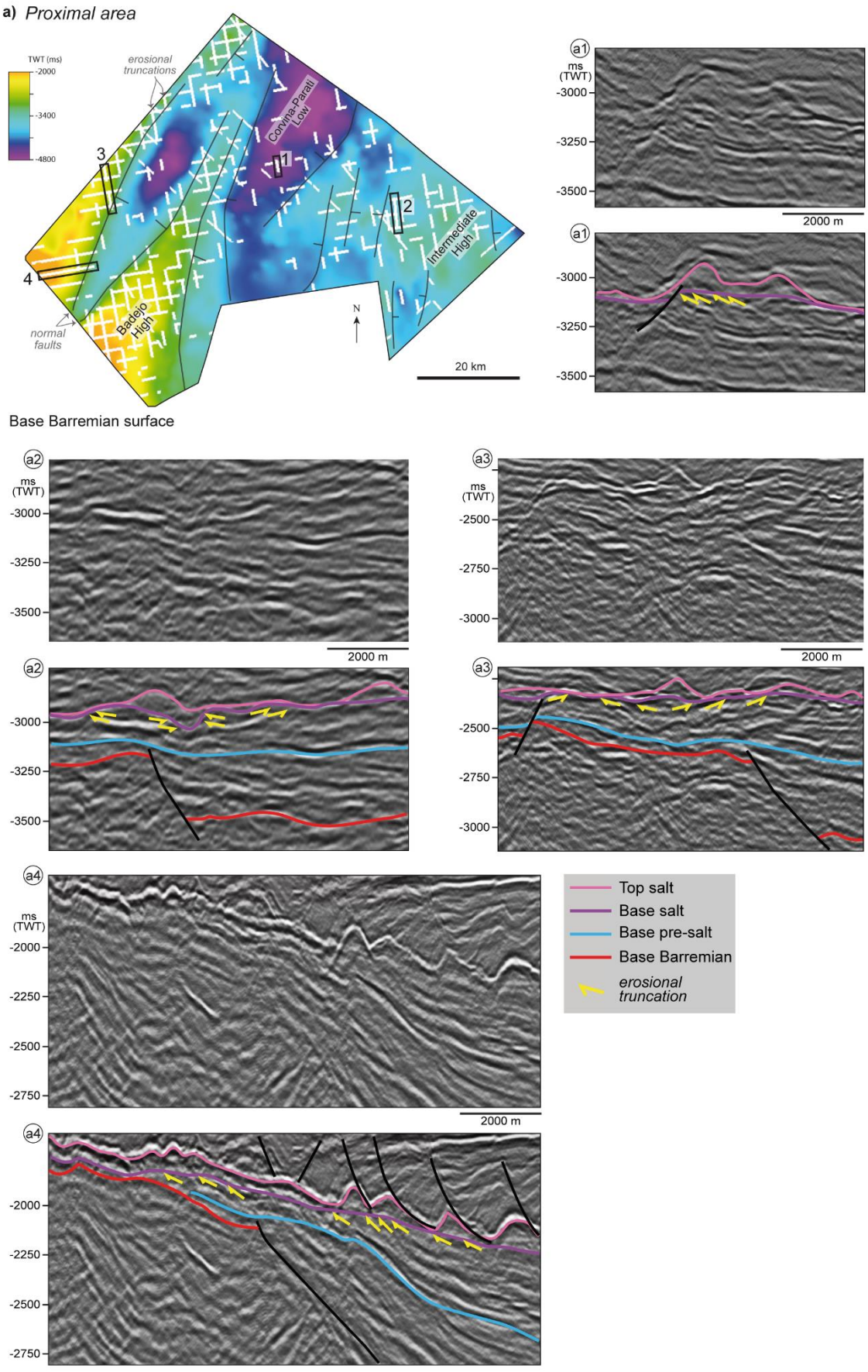
a) Proximal area
TWT (ms)
-2000
-3400
-4800
erosional truncations
Corvina-Parati Low
Intermediate High
Badejo High
normal faults
N
20 km
Base Barremian surface
a1
ms (TWT)
-3000
-3250
-3500
2000 m
a2
-3000
-3250
-3500
a3
-2500
-2750
-3000
a4
-2000
-2250
-2500
-2750
Top salt
Base salt
Base pre-salt
Base Barremian
erosional truncation

119

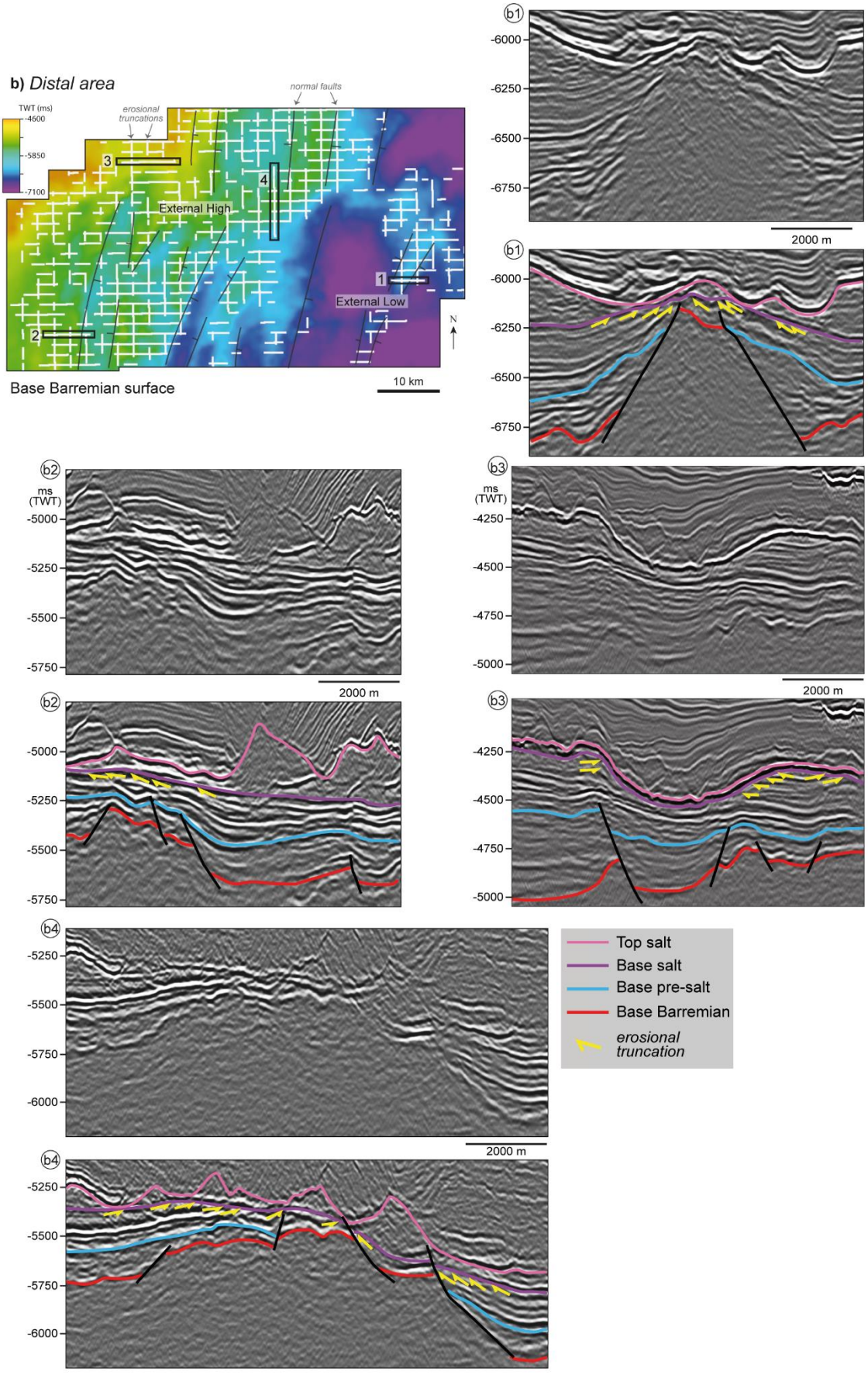
b) Distal area
normal faults
TWT (ms)
-4600
-5850
-7100
erosional truncations
3
4
External High
1
External Low
2
N
Base Barremian surface
10 km
b1
-6000
-6250
-6500
-6750
2000 m
b2
ms (TWT)
-5000
-5250
-5500
-5750
b3
-4250
-4500
-4750
-5000
b4
-6000
Top salt
Base salt
Base pre-salt
Base Barremian
erosional truncation

120

(previous pages) **Figure 10**. Time map of the base-rift (top Cabiúnas Formation) surface in the proximal (a) and distal (b) areas, with series of erosional truncations mapped in white. Numbers 1 to 4 are segments of seismic lines to best show the reflection terminations, highlighted in yellow arrows when they are erosional truncations.

7. Discussions

7.1. Expression and development of unconformities in the Campos Basin

There are three key seismic-scale stratigraphic surfaces identified below Aptian salt in the Campos Basin. The oldest one, the base-Barremian surface (c. 130 Ma), separates the volcanics of Cabiúnas Fm. and pre-rift basement rocks from early syn-rift sedimentary strata (Winter et al., 2007) (Figures 1, 2 and 5). This surface post-dates the syn-rift unconformity (*sensu* Bosence, 1998) or rift onset unconformity (*sensu* Falvey, 1974), located either within or at the base of the Cabiúnas Formation (Goldberg et al., 2017). We now discuss the character and potential origin of the two younger unconformities that define the base-pre-salt and the base-salt.

7.1.1. *Base-pre-salt unconformity*

Across basement highs the base-pre-salt surface is an erosional unconformity that is onlapped by the overlying reflections, but that passes laterally into a correlative conformity in adjacent depocentres (Figures 7 and 9). The base-pre-salt is thus classified as an angular unconformity, separating divergent and locally deformed reflections of the Barremian – lower Aptian from subparallel reflections of the upper Aptian. This unconformity has been previously documented in the Campos, Santos and Espírito Santo basins, where it was referred to as the *pre-Alagoas* (or *pre-neo-Alagoas*) unconformity (c. 120 – 123 Ma) (Guardado et al., 1989; Winter et al., 2007; Mohriak et al., 2008). Our well data show that this surface coincides with the base of the Alagoas Stage (123 Ma) (Figure 5).

Some authors argue that the pre-Alagoas unconformity corresponds to the breakup unconformity (e.g. Cainelli and Mohriak, 1999; Mohriak et al., 2008), which Bosence (1998) positions at the syn- to post-rift contact. This interpretation leads to the classification of the upper Aptian of the southeastern Brazilian basins as *transitional* or *post-rift* (e.g. Rangel et al., 1994; Cainelli and Mohriak, 1999; Beglinger et al., 2012; Alvarenga et al., 2021). The term *breakup unconformity* as defined by Falvey (1974) is a basin-wide erosional surface, originating from the uplift of rift flanks at the time of breakup, and synchronous with the onset of oceanic crust accretion. This unconformity is typically described as being erosional, truncating underlying, wedge-shaped, syn-rift strata, separating them from younger post-rift sequences that show little to no evidence of fault-controlled deposition (Braun and Beaumont, 1989; Franke, 2013). The breakup unconformity thus represents the cessation (or decrease) of rift-related tectonic subsidence, and the onset of a long-wavelength, relatively slow subsidence driven by post-rift cooling of the newly formed oceanic crust (Hiscott et al. 1990).

More recently, multistage models of continental breakup have been developed, using a combination of observations from new, higher-resolution geophysical data imaging the distal parts of rifted margins, and exposures of exhumed, ancient margins now preserved in mountain belts. These models argue that the process of continental breakup is variably distributed in time and space, and thus is not recorded by a single surface (or reflection) that is age-equivalent across the proximal and distal domains of rifted margins (e.g. Peron-Pindivic et al., 2013; Brune et al., 2014; Pérez-Gussinyé, 2020; Chenin et al., 2021). According to Pérez-Gussinyé et al. (2020), on weak asymmetric margins such as the Angola/Northern Campos-Espirito Santo conjugates, the breakup event is only recorded as an unconformity in areas affected by deformation related to final crustal rupture (i.e. the most distal part of the margin). This is the cessation of tectonic

subsidence does not occur simultaneously across the entire margin, and thus it does not generate a basin-wide response recorded as a stratigraphic marker across the entire basin. Instead, margin breakup generates local flexural rebounds in response to elastic stress drops linked with progressive faulting and thinning (Pérez-Gussinyé et al., 2020). Chenin et al. (2021) state that not all unconformities within rift basins mark the beginning of the post-rift. For example, the proximal domains of rifts may contain unconformities related to local or large-scale tectonic events, or due to climatic events or changes in sea-level (Prosser, 1993). Previous studies also show that rather than a rapid tectonic event, lithospheric breakup reflects a gradual process where extension of exhumed upper mantle (and continental crust) and emplacement of normal oceanic crust may occur simultaneously until the later becomes predominant (Sibuet et al., 2007; Jagoutz et al., 2007).

We thus argue that the base-pre-salt (or *pre-neo-Alagoas*) unconformity predates and is thus not related to the breakup event associated with formation of the South Atlantic; this interpretation is consistent with other studies of marginal basins of SE Brazil (e.g. Karner and Gamboa, 2007; Torsvik et al., 2009). We instead interpret that this surface is a *rift migration unconformity* (*sensu* Pérez-Gussinyé et al., 2020) formed when deformation across a given fault block (and slip on its bounding faults) ceases and migrates oceanward. It is therefore an angular unconformity separating syn- and post-tectonic strata, rather than syn- and post-rifting strata (*sensu* Péron-Pinvidic et al., 2007), marking the onset of a sag-type basin. Even though the base-pre-salt unconformity is identified in both the proximal and distal areas of Campos Basin, it is diachronous across the basin, reflecting the oceanward migration of deformation (Ranero and Pérez-Gussinyé, 2010; Pérez-Gussinyé et al., 2020). In the distal portion of our study area, this unconformity marks the end of fault activity, although, a few rift-related faults remained

active locally after its development (numbered faults in Figure 9). Chenin et al. (2015) uses the term *necking unconformity* for the transition from syn- to post-tectonic deposits. The unconformity described here may thus be called the necking unconformity and may thus record a period of substantial and more distributed crustal thinning (Peron-Pinvidic and Manatschal, 2009; Mohn et al., 2010).

7.1.2. *Base-salt unconformity*

The contact between the salt and the pre-salt strata is rugose in most parts, being underlain by either concordant reflections or reflections that are erosionally truncated (Figures 7, 9 and 10). The related unconformity is regional, being more developed on basement highs across the margin. Between the Intermediate/External highs and the External Low, the unconformity is expressed as a downcutting erosional unconformity (Figure 5), which indicate either: (1) vertical erosion into sub-horizontal strata or, perhaps more likely given the tectonic history of the margin; (2) the External Low tilted oceanward after salt deposition, meaning this is an *apparently* downcutting erosional unconformity that originally formed by erosion of already tilted strata. Within basement lows, concordant reflections dominate, but there are some truncations (especially in the proximal area) that due to their spatial restriction are likely associated to either: (1) normal faults that were active prior to salt deposition (Figures 7a and 10 a1) or more speculatively; (2) lacustrine wave erosion (where the is no fault near the erosion, e.g. Figure 7b to NE).

The salt – pre-salt contact is classified as an unconformity (*sensu* Stokes, 1982) given the regional character of the surface, and based on the fact it defines an abrupt shift in depositional environment from isolated lacustrine to a more extensive, but still

restricted marine system (Winter et al., 2007). The period of erosion and nondeposition that this surface comprehends is uncertain. The estimated age of the evaporites is c. 110 – 116 Ma (Szatmari et al., 2021), and that the estimated duration of evaporite deposition is c. 0.5 Ma – based on correlation of the main evaporite sequences to Milankovitch cycles (Freitas, 2006) and on the comparison to known evaporite depositional rates in different salt basins (Davison et al., 2012). This means that base-salt unconformity comprehends a time gap of c. <0.1–6.0 Ma, given salt deposited for 0.5 Ma and that deposition could have started anytime between c. 110 and 116 Ma.

Alves et al. (2017) also document base-salt erosion in the Santos Basin. These authors attribute this erosion to three factors, depending on the specific structural position in which it is observed. For example, on structural highs, similar to what we observe in our study, the authors associate erosion with sub-aerial exposure. In contrast, some distance (i.e., up to 20 km) from structural highs they attribute erosion to either (1) thick-skinned tectonics that caused diachronous reactivation and inversion of rift-related normal faults; or (2) drag (i.e., friction) along the top of the sub-salt strata where it is in contact with the overriding, basinward-flowing salt. They propose that the latter mechanism is specifically relevant where the top pre-salt is flat and subsalt strata are strongly eroded (see their figure 9). Alves et al. (2017) also quantified the magnitude of base-salt erosion, suggesting this locally exceeded 20% (c. 62 m) of the pre-salt Aptian carbonate original thickness (313 m – Moreira et al., 2007). To derive this value the authors use the method of Roberts and Yielding (1991), where reflection truncations are mapped across eroded half-grabens and projected upwards following a tabular and regular geometry (see their figure 6). A key question arising from this interpretation is, therefore, "does basinward-flowing salt have sufficient mechanical strength to erode large volumes

of underlying material, which in the case of Campos and Santos basins are lithified carbonates?".

There are two end-members of flow regimes for salt; Poiseuille and Couette (e.g Rowan et al., 2004; Weijermars et al., 2014; Fossen, 2016; Sarkarinejad et al., 2018). Poiseuille flow is driven by a lateral pressure gradient within the salt; in this case, overburden strata that load the salt and drive deformation may subside into the salt, but it does not move horizontally. Couette flow is dominated by shear stress and occurs when the sedimentary overburden glides down a gentle slope. In nature, it is likely that salt flow is a mix of both (i.e. hybrid Couette-Poiseuille flow; e.g. Sarkarinejad et al., 2018 - see their figure 1). In all three flow regimes (Couette, Poiseuille and hybrid), the salt velocity during horizontal translation is null at the base-salt, meaning the salt (and overburden) movement is decoupled from the underlying strata and we argue, cannot therefore erode it. Furthermore, if salt had eroded the underlying rocks, there should be evidence of pre-salt-derived clastics and carbonates within the salt. We see no evidence of this, at least at the seismic-scale. Finally, in the Campos Basin there is no relation between the style of salt and overburden structures and pre-salt erosion. More specifically, rather that intra-salt and overburden shortening structures being restricted to subsalt highs (see Alves et al., 2017), areas with pronounced pre-salt erosion are characterized by extensional salt structures (Figures 7 and 9) developed on structural highs as salt flowed oceanward.

Karner and Gamboa (2007) have identified an unconformity in the salt – pre-salt contact across the entire Aptian salt basin, including the Santos, Campos and Espírito Santo basins in Brazil, and their conjugate basins in West Africa. The authors attribute the origin of this unconformity to be a lake level relative fall during the mid-late Aptian, triggered by a climate change. In the West African basins, the authors estimated at least 500 – 650 m of erosion measuring canyon cutting and incisions in early-mid Aptian

clinoforms. Karner and Gamboa (2007) also suggest that rift-related normal faults were locally active during salt deposition in the Santos Basin, offsetting the base of the salt, and causing block uplift and erosion within basement lows.

Based on the above observations and in contrast to Alves et al. (2017), we argue that the base-salt unconformity formed *before* rather than after salt deposition. We suggest that the unconformity formed in response to base-level fall within a lacustrine environment (also stated by Karner and Gamboa, 2007), an interpretation supported by the presence of channel-like incision into the top of the pre-salt succession (e.g. Figure 10 b3). The unconformity is regional in extent due to the shallow bathymetry at that time, although the magnitude of incision may have been locally enhanced by local uplift around active faults, especially in the distal area. Geodynamic models for the South Atlantic salt basins provide different potential explanations for the origin of this uplift. First, Karner and Gamboa (2007) suggest that heat advected during lithospheric thinning kept the middle - upper Aptian at relatively shallow depths. Second, Huismans and Beaumont (2011) propose that a widespread shallow bathymetry requires an isostatic balance with sub-crustal emplacement of hot depleted lower-cratonic lithosphere, which is less dense than upwelled asthenosphere. Finally, Huismans and Beaumont (2014) use numerical models to demonstrate that counterflow of cratonic lithosphere can cause exposure of large regions of continental lithosphere in the outer region of a margin.

7.2. Stratigraphic expression of the syn- and post-rift stages of the Campos Basin

The Barremian – lower Aptian interval is characterized by divergent reflections contained within wedge-shaped packages that expand towards rift-related normal faults. Such growth strata record fault activity, and, for that reason, are classified as syn-tectonic

(Péron-Pinvidic et al., 2007) *and* syn-rift (Masini et al., 2013). The unconformity capping these strata record a time when rifting had migrated oceanward, but not to such an extent that all inboard faults were inactive in the distal area (see previous item; Figure 9).

The upper Aptian pre-salt interval is composed of subparallel and relatively continuous reflections that are locally divergent, but which are typically contained within lenticular packages that thickens towards the centre of basement lows. The base of this succession contains reflections that onlap basement highs or the base-pre-salt surface, indicating an increase in depositional area when compared to the underlying interval. Based on the age constraints most accepted in the literature (i.e., c. 123 – 116 Ma; Karner and Gamboa 2007; Winter et al., 2007), the pre-salt interval can be classified as syn-rifting, given it is pre-breakup (c. 115 Ma, Heine et al., 2013). The aforementioned seismic-stratigraphic characteristics of the pre-salt interval indicate it is post-tectonic at a margin scale, although locally, it can also be syn-tectonic, i.e., faulted and/or exhibit thickening towards a few normal faults.

The origin of a late-rift sag basin characterized by limited upper crustal faulting and shallow water depths can be explained by depth-dependent extension (Karner and Gamboa, 2007; Huismans and Beaumont, 2011; Huismans and Beaumont, 2014). Karner and Gamboa (2007) suggest that depth-dependent extension during the late Aptian on the West African and Brazilian margins caused greater thinning of the lower crust and underlying lithosphere when compared to the upper crust. This mechanism generated sufficient accommodation for the deposition of the upper Aptian pre-salt sequence and the c. 2 km-thick evaporite sequence itself (Karner and Gamboa, 2007). Other possible depth-dependent mechanisms are sub-crustal emplacement of hot depleted lower-cratonic lithosphere (Huismans and Beaumont, 2011), or counterflow of cratonic lithosphere (Huismans and Beaumont, 2014).

Based on the age constraints most accepted in the literature for salt deposition, (110 – 116 Ma; Moreira et al., 2007; Gamboa et al., 2008; Szatmari et al., 2021), and for the continental breakup in southern Campos Basin (c. 115 Ma – Heine et al., 2013; Moulin et al., 2013), the salt could be syn- to post-rift, given it could be pre-, syn- or post-breakup. However, considering what is most accepted in works that address the South Atlantic evolution, salt deposition was synchronous in both West Africa and SE Brazil margins, being pre- to syn-breakup (e.g. Karner and Gamboa, 2007; Torsvik et al., 2009; Heine et al., 2013; Kukla et al., 2018; Pérez-Gussinyé, 2020; Szatmari et al., 2021). This means that the upper Aptian salt is syn-rifting.

We also show that the classical models of rift basins that use the geometry and seismic facies of the sedimentary units in order to classify distinct tectono-stratigraphic stages (e.g. Prosser, 1993; Bosence, 1998; Gawthorpe and Leeder, 2000) work well to describe the filling of individual half-grabens, but cannot be applied to rifted margins, such as Campos Basin. Due to the limited geophysical imaging available in the past, these models were based on the acquisition of data from one or only several adjacent basins exposed in the field or imaged in the subsurface (Peron-Pinvidic and Manatschal, 2019). Consequently, little was known about the structure and stratigraphy of the distal domains of rift systems. Improvements in seismic imaging, analytical methods, and computing capabilities, combined with deep sea drilling showed that the distal domains of rifted margins are different from the proximal ones, and new concepts and models emerged. Modern concepts now include polyphase (or multiphase) rifting, rift domain names (e.g. necking domain) and migration of deformation (e.g. Ranero and Pérez-Gussinyé, 2010; Brune et al., 2014; Pérez-Gussinyé et al., 2020; Chenin et al., 2021). This new terminology is still debated, and it is clear that terms such as syn-rift, post-rift, and breakup unconformity need to be revised (Masini et al., 2013).

8. Conclusions

We use 2D and 3D seismic reflection and borehole data from the south-central Campos Basin to discuss the syn- to post-rift transition. The key conclusions of our study are:

1. We identified four key stratigraphic surfaces in the study area, which define three intervals with distinct geometries and seismic facies filling rift-related topography in Campos Basin: Barremian – lower Aptian, upper Aptian pre-salt and salt.
2. The Barremian – lower Aptian interval is characterized by divergent reflections composing syn-rift, syn-tectonic continental lake deposits, thickening towards graben and half-graben-bounding normal faults. This stage ends with the development of an angular unconformity (mid-Aptian; pre-neo-Alagoas) that records a time when rifting had migrated oceanward.
3. The upper Aptian pre-salt interval is typically defined of subparallel and relatively continuous reflections composing a broadly lenticular geometry that thickens towards the centre of basement lows, but that locally diverge towards rift-related normal faults, being characterized as syn-rifting and post-tectonic. This unit is bounded by an erosional unconformity identified on and adjacent to basement highs, which is inferred to have formed due to base-level fall and uplift associated with local fault reactivation.
4. The upper Aptian salt interval is characterized by salt welds and structures that record the horizontal translation of salt and its overburden. The top-salt is a concordant surface with the overlying Albian carbonates.
5. Based on the geometries and seismic facies of each interval, we conclude that the Barremian – lower Aptian is syn-rift and syn-tectonic, and the upper Aptian is

syn-rift and post-tectonic. The two intervals are separated by a rift migration unconformity that predates and is not related to the breakup event.

Acknowledgments

F.B. Amarante thanks CNPq (National Council for Scientific and Technological Development of Brazil) for the doctorate scholarship. The authors gratefully acknowledge ANP (Brazil's National Oil, Natural Gas and Biofuels Agency) for providing the data and for the license to publish this article.

References

Abrahão, D., Warme, J.E., 1990. Lacustrine and associated deposits in a rifted continental margin e lower cretaceous Lagoa Feia formation, Campos Basin, offshore Brazil. In: Katz, B.J. (Eds.), Lacustrine Basin Exploration: Case Studies and Modern Analogs. AAPG 50, 287–305.

Allen, P.A., Allen, J.R. 2005. Basin analysis: principles and applications. (second ed.), Wiley-Blackwell Publishing, Sydney, p. 560

Alvarenga, R.d.S., Kuchle, J., Iacopini, D., Goldberg, K., Scherer, C.M.d.S., Pantopoulos, G., Ene, P.L., 2021. Tectonic and Stratigraphic Evolution Based on Seismic Sequence Stratigraphy: Central Rift Section of the Campos Basin, Offshore Brazil. Geosciences 11, 338. https://doi.org/10.3390/geosciences11080338

Alves, T.M., Fetter, M., Lima, C., Cartwright, J.A., Cosgrove, J., Gangá, A., Queiroz, C.L., Strugale, M., 2017. An incomplete correlation between pre-salt topography, top reservoir erosion, and salt deformation in deep-water Santos Basin (SE Brazil). Marine and Petroleum Geology 79, 300–320. https://doi.org/10.1016/j.marpetgeo.2016.10.015

Amarante, F.B., Jackson, C.A., Pichel, L.M., Scherer, C.M.S., Kuchle, J., 2021. Pre-salt rift morphology controls salt tectonics in the Campos Basin, offshore SE Brazil. Basin Research 33 (5), 2837–2861. https://doi.org/10.1111/bre.12588

Amarante, F.B., Kuchle, J., Iacopini, D., Scherer, C.M.S., Alvarenga, R.S., Ene, P.L., Schilling, A.B., 2020. Seismic tectono-stratigraphic analysis of the Aptian pre-salt marginal system of

396 Espírito Santo Basin, Brazil. Journal of South American Earth Sciences 98, 102474.
397 https://doi.org/10.1016/j.jsames.2019.102474

398 Baksi, A.K., 2018. Paraná flood basalt volcanism primarily limited to ~ 1 Myr beginning at 135
399 Ma: New 40 Ar/ 39 Ar ages for rocks from Rio Grande do Sul, and critical evaluation of published
400 radiometric data. Journal of Volcanology and Geothermal Research 355, 66–77.
401 https://doi.org/10.1016/j.jvolgeores.2017.02.016

402 Beglinger, S.E., Doust, H., Cloetingh, S., 2012. Relating petroleum system and play development
403 to basin evolution: West African South Atlantic basins. Marine and Petroleum Geology 3, 1–25.

404 Bosence, D.W.J., 1998. Stratigraphic and sedimentological models of rift basins. In: Purser, B.H.,
405 Bosence, D.W.J. (Eds.), Sedimentation and Tectonics of Rift Basins: Red Sea, Gulf of Aden.
406 London: Chapman e Hall. 9–25.

407 Bott, M.P.H., 1995. Rifted passive margins. In: Olsen, K.H. (Eds.) Continental Rifts: Evolution,
408 Structure, Tectonics. Developments in Geotectonics 25, 409–426

409 Braun, J., Beaumont, C., 1989. A physical explanation of the relation between flank uplifts and
410 the breakup unconformity at rifted continental margins. Geology 17, 760–764.

411 Bruhn, C.H.L., Gomes, J.A.T., Del Lucchese, C., Jr., Johann, P.R.S., 2003. Campos Basin:
412 Reservoir Characterization and Management - Historical Overview and Future Challenges, in:
413 Offshore Technology Conference. Presented at the Offshore Technology Conference, Offshore
414 Technology Conference. https://doi.org/10.4043/15220-ms

415 Brune, S., Heine, C., Pérez-Gussinyé, M., Sobolev, S.V., 2014. Rift migration explains
416 continental margin asymmetry and crustal hyper-extension. Nature Communications 5, 4014.

417 Cainelli, C., Mohriak, W.U., 1999. Some remarks on the evolution of sedimentary basins along
418 the eastern Brazilian continental margin. Episodes, 22 (3), 206–216.

419 Cartwright, J., 1991. The kinematic evolution of the Coffee Soil Fault. Geological Society,
420 London, Special Publications 56, 29–40.

421 Chang, H.K., Kowsmann, R.O., Figueiredo, A.M.F., Bender, A., 1992. Tectonics and stratigraphy
422 of the East Brazil rift system: an overview. Tectonophysics 213, 97–138.

Chenin, P., Manatschal, G., Ghienne, J., Chao, P., 2021. The syn-rift tectono-stratigraphic record of rifted margins (Part II): A new model to break through the proximal/distal interpretation frontier. Basin Research 00, 1–44. https://doi.org/10.1111/bre.12628

Chenin, P., Manatschal, G., Lavier, L.L., Erratt, D., 2015. Assessing the impact of orogenic inheritance on the architecture, timing and magmatic budget of the North Atlantic rift system: A mapping approach. Journal of the Geological Society of London, 172, 711–720. https://doi.org/10.1144/jgs20 14-139

Davison, I., 2007. Geology and tectonics of the South Atlantic Brazilian salt basins. Geological Society, London, Special Publications 272, 345–359. https://doi.org/10.1144/gsl.sp.2007.272.01.18

Davison, I., Anderson, L., Nuttall, P., 2012. Salt deposition, loading and gravity drainage in the Campos and Santos salt basins. Geological Society, London, Special Publications 363, 159–174. https://doi.org/10.1144/sp363.8

Dias, J.L., Oliveira, J.Q., Vieira, J.C., 1988. Sedimentological and stratigraphyc analysis of the Lagoa Feia Formation, rift phase of Campos Basin, offshore Brazil. Revista Brasileira de Geociências 18 (3), 252–260.

Dooley, T.P., Hudec, M.R., Carruthers, D., Jackson, M.P.A., Luo, G., 2017. The effects of base-salt relief on salt flow and suprasalt deformation patterns — Part 1: Flow across simple steps in the base of salt. Interpretation 5, SD1–SD23. https://doi.org/10.1190/int-2016-0087.1

Falvey, D., 1974. The development of continental margins in plate tectonic theory. J. Aust. Pet. Explor. Assoc. 14, 95–106.

Fetter, M., 2009. The role of basement tectonic reactivation on the structural evolution of Campos Basin, offshore Brazil: Evidence from 3D seismic analysis and section restoration. Marine and Petroleum Geology 26, 873–886. https://doi.org/10.1016/j.marpetgeo.2008.06.005

Freitas, R.T.J., 2006. Ciclos deposicionais evaporiticos da bacia de Santos: una analise cicloestratigrafica a partir de dados de 2 poços e de traços de sísmica. Masters thesis, Instituto de Geociencias, Universidade Federal do Rio Grande do Sul, Brazil.

Gamboa, L.A.P., Machado, M.A.P., Silviera, D.P., Freitas, J.T.R., Silva, S.R.P., 2008. Evaporitos estratificados no Atlântico Sul: interpretação sísmica e controle tectono-estratigráfico na Bacia de

452 Santos. In: Mohriak, W., Szatmari, P., Anjos, S.M.C. (Eds.) Sal: Geologia e Tectonica. Editora
453 Beca, São Paulo, Brazil, 340–359.

454 Gawthorpe, R.L., Leeder, M.R., 2000. Tectono-sedimentary evolution of active extensional
455 basins. Basin Research 12, 195–218.

456 Goldberg, K., Kuchle, J., Scherer, C.M.S., Alvarenga, R.S., Ene, P.L., Armelenti, G., De Ros,
457 L.F., 2017. Re-Sedimented deposits in the rift section of the Campos Basin. Marine and Petroleum
458 Geology 80, 412–431.

459 Guardado, L.R., Gamboa, L.A.P., Lucchesi, C.F., 1989. Petroleum geology of Campos Basin,
460 Brazil: a model for producing Atlantic type basin. In: Edwards, J.D., Santagrossi, P.A. (Eds.),
461 Divergent/Passive Margins Basins. AAPG Memoir 48, 3–36.

462 Guardado, L.R., Spadini, A.R., Brandão, J.S.L., Mello, M.R., 2000. Petroleum system of the
463 Campos Basin, Brazil. In: Mello, M.R., Katz, B.J. (Eds.), Petroleum Systems of South Atlantic
464 Margins. AAPG Memoir 73, 317–324.

465 Heine, C., Zoethout, J., Müller, R. D., 2013. Kinematics of the South Atlantic rift. Solid Earth,
466 4(2), 215–253. https://doi.org/10.5194/se-4-215-2013

467 Hiscott, R.N., Wilson, R.C.L., Gradstein, F.M., Pujalte, V., Garcia-Mondejar, J., Boudreau,
468 R.R.D. Wishart, H.A., 1990. Comparative stratigraphy and subsidence history of Mesozoic rift
469 basins of North Atlantic. American Association of Petroleum Geologists Bulletin 74, 60–76.

470 Huismans, R.S., Beaumont, C., 2014. Rifted continental margins: The case for depth-dependent
471 extension. Earth and Planetary Science Letters 407, 148–162.
472 https://doi.org/10.1016/j.epsl.2014.09.032

473 Huismans, R.S., Beaumont, C., 2011. Depth-dependent extension, two-stage breakup and cratonic
474 underplating at rifted margins. Nature 473, 74–78. http://dx.doi.org/10.1038/nature09988

475 Issler, D., McQueen, H., Beaumont, C. 1989. Thermal and isostatic consequences of simple shear
476 extension of the continental lithosphere. Earth and Planetary Science Letters 91, 341–358.

477 Jagoutz, O., Müntener, O., Manatschal, G., Rubatto, D., Péron-Pinvidic, G., Turrin, B.D., Villa,
478 I.M., 2007. The rift-to-drift transition in the North Atlantic: A stuttering start of the MORB
479 machine? Geology, 35, 1087–1090.

480 Jackson, M.P.A., Cramez, C. & Fonck, J-M., 2000. Role of subaerial volcanic rocks and mantle
481 plumes in creation of South Atlantic margins: implications for salt tectonics and source rocks,
482 Marine and Petroleum Geology 17, 477–498.

483 Karner, G.D., Gamboa, L.A.P., 2007. Timing and origin of the South Atlantic pre-salt sag basins
484 and their capping evaporates. In: Schreiber, B.C., Lugli, S., Babel, M. (Eds.) Evaporites through
485 Space and Time. Geological Society, London, Special Publications 285, 15–35.

486 Kuchle, J., Scherer, C.M.S., 2010. Sismoestratigrafia de bacias rifte: técnicas, métodos e sua
487 aplicação na Bacia do Recôncavo. Boletim de Ciências da Petrobrás 18 (2), 179–206.

488 Kukla, P.A., Strozyk, F., Mohriak, W.U., 2018. South Atlantic salt basins – Witnesses of
489 complex passive margin evolution. Gondwana Research 53, 41–57.
490 https://doi.org/10.1016/j.gr.2017.03.012

491 Manatschal, G., Chenin, P., Ghienne, J.-F., Ribes, C., Masini, E., 2022. The syn-rift tectono-
492 stratigraphic record of rifted margins (Part I): Insights from the Alpine Tethys. Basin Research
493 34, 457– 488. https://doi.org/10.1111/bre.12627

494 Masini, E., Manatschal, G., Mohn, G., 2013. The Alpine Tethys rifted margins: Reconciling old
495 and new ideas to understand the stratigraphic architecture of magma-poor rifted margins.
496 Sedimentology 60, 174–196. https://doi.org/10.1111/sed.12017

497 Mohn, G., Manatschal, G., Müntener, O., Beltrando, M., Masini, E., 2010. Unravelling the
498 interaction between tectonic and sedimentary processes during lithospheric thinning in the Alpine
499 Tethys margins. International Journal of Earth Sciences 99, 75–101.

500 Mohriak, W., Nemčok, M., Enciso, G., 2008. South Atlantic divergent margin evolution: rift-
501 border uplift and salt tectonics in the basins of SE Brazil. Geological Society, London, Special
502 Publications 294, 365–398. https://doi.org/10.1144/sp294.19

503 Moreira, J.L.P., Madeira, C.V., Gil, J.A., Machado, M.A.P., 2007. Bacia de Santos. Boletim da
504 Geociências da Petrobras, Rio de Janeiro, 15, 531–549.

505 Morley, C.K., 2002. Evolution of large normal faults: Evidence from sesmic refletion data. AAPG
506 Bulletin 86 (6), 961–978.

507 Moulin, M., Aslanian, D., Unternehr, P., 2010. A new starting point for the South and Equatorial
508 Atlantic Ocean. Earth-Science Reviews 98, 1–37.

Moulin, M., Aslanian, D., Rabineau, M., Patriat, M., Matias, L., 2013. Kinematic keys of the Santos–Namibe basins. Geological Society, London, Special Publications 369, 91–107. https://doi.org/10.1144/sp369.3

Nottvedt, A., Gabrielsen, R.H., Steel, R.J., 1995. Tectonostratigraphy and sedimentary architecture of rift basins, with reference to the northern North Sea. Marine and Petroleum Geology 12 (8), 881–901. https://doi.org/10.1016/0264-8172(95)98853-w

Pérez-Gussinyé, M., Andrés-Martínez, M., Araújo, M., Xin, Y., Armitage, J., & Morgan, J. P., 2020. Lithospheric strength and rift migration controls on synrift stratigraphy and breakup unconformities at rifted margins: Examples from numerical models, the Atlantic and South China Sea margins. Tectonics, 39, e2020TC006255. https://doi.org/10.1029/2020TC006255

Péron-Pinvidic, G., Manatschal, G., Minshull, T.A., Sawyer, D.S., 2007. Tectonosedimentary evolution of the deep Iberia-Newfoundland margins: Evidence for a complex breakup history. Tectonics 26(2), TC2011.

Péron-Pinvidic, G., Manatschal, G., 2009. The final rifting evolution at deep magma-poor passive margins from Iberia–Newfoundland: a new point of view. International Journal of Earth Sciences 98, 1581–1597.

Péron-Pinvidic, G., Manatschal, G., Osmundsen, P.T., 2013. Structural comparison of archetypal Atlantic rifted margins: A review of observations and concepts. Marine and Petroleum Geology 43, 21–47. https://doi.org/10.1016/j.marpetgeo.2013.02.002

Peron-Pinvidic, G., Manatschal, G., 2019. Rifted Margins: State of the Art and Future Challenges. Frontiers in Earth Sciences 7:218. https://doi.org/10.3389/feart.2019.00218

Prosser, S., 1993. Rift-related linked depositional systems and their seismic expression. In: Williams, G.D., Dobb, A. (Eds.), Tectonics and Seismic Sequence Stratigraphy. Geological Society of London, London, Special Publication 71, 35–66.

Quirk, D.G., Hertle, M., Jeppesen, J.W., Raven, M., Mohriak, W.U., Kann, D.J., Nørgaard, M., Howe, M.J., Hsu, D., Coffey, B., Mendes, M.P., 2013. Rifting, subsidence and continental break-up above a mantle plume in the central South Atlantic. Geological Society, London, Special Publications 369, 185–214. https://doi.org/10.1144/sp369.20

Ranero, C.R., Pérez-Gussinyé, M., 2010. Sequential faulting explains the asymmetry and extension discrepancy of conjugate margins. Nature 468, 294–299.

https://doi.org/10.1038/nature09520

Rangel, H.D., Martins, F.A.L., Esteves, F.R., Feijó, F.J., 1994. Bacia de Campos. Boletim de Geociências da Petrobras 8 (1), 203–218.

Roberts, A.M., Yielding, G., 1991. Deformation around basin-margin faults in the North Sea/mid-Norway rift. Geological Society, London, Special Publications 56, 61–78. https://doi.org/10.1144/gsl.sp.1991.056.01.05

Rowan, M.G., Peel, F.J., Vendeville B.C., 2004, Gravity-driven fold belts on passive margins. In McClay, K.K. (Eds.), Thrust tectonics and hydrocarbon systems: AAPG Memoir 82, 157–182.

Sibuet, J.C., Srivastava, S., Manatschal, G., 2007. Exhumed mantle-forming transitional crust in the Newfoundland-Iberia rift and associated magnetic anomalies. Journal of Geophysical Research 112, B06105.

Stokes, W.L., 1982. Essentials of Earth History 4th Edition. Prentice Hall Inc, 65 p. ISBN 0-13-285890-8

Strugale, M., Cartwright, J., 2022. Tectono-stratigraphic evolution of the rift and post-rift systems in the Northern Campos Basin, offshore Brazil. Basin Research 00, 1–33. https://doi.org/10.1111/bre.12674

Szatmari, P., 2000. Habitat of petroleum along the South Atlantic margins. In: Mello, M.R., Katz, B.J. (Eds.), Petroleum Systems of South Atlantic Margins: AAPG Memoir 73, 69–75.

Szatmari, P., de Lima, C. M., Fontaneta, G., de Melo Lima, N., Zambonato, E., Menezes, M. R., Bahniuk, J., Coelho, S. L., Figueiredo, M., Florencio, C. P., 2021. Petrography, geochemistry and origin of South Atlantic evaporites: The Brazilian side. Marine and Petroleum Geology, 127, 104805. https://doi.org/10.1016/j.marpe tgeo.2020.104805

Tedeschi, L. R., Jenkyns, H. C., Robinson, S. A., Lana, C. C., Menezes Santos, M. R. F., Tognoli, F. M. W., 2019. Aptian carbon-isotope record from the Sergipe-Alagoas Basin: New insights into oceanic anoxic event 1a and the timing of seawater entry into the South Atlantic. Newsletters on Stratigraphy, 53, 529. https://doi.org/10.1127/nos/2019/0529

Torsvik, T.H., Rousse, S., Labails, C., Smethurst, M.A., 2009. A new scheme for the opening of the South Atlantic Ocean and the dissection of an Aptian salt basin. Geophysical Journal International 177, 1315–1333.

568 Weijermars, R., Jackson, M.P.A., Dooley, T.P., 2014. Quantifying drag on wellbore casings in
569 moving salt sheets. Geophysical Journal International 198, 965–977.

570 Winter, W.R., Jahnert, R.J., França, A.B., 2007. Bacia de Campos. Boletim de Geociências da
571 Petrobras 15(2), 511–529.